BABAR-PUB-08/016
SLAC-PUB-13341
arXiv:0807.4974
Revised--January 2009

Measurements of $\mathcal{B}(\overline{B}^0 \to \Lambda_c^+ \overline{p})$ and $\mathcal{B}(B^- \to \Lambda_c^+ \overline{p}\pi^-)$ and Studies of $\Lambda_c^+\pi^-$ Resonances

B. Aubert,[1] M. Bona,[1] Y. Karyotakis,[1] J. P. Lees,[1] V. Poireau,[1] E. Prencipe,[1] X. Prudent,[1] V. Tisserand,[1] J. Garra Tico,[2] E. Grauges,[2] L. Lopez[ab],[3] A. Palano[ab],[3] M. Pappagallo[ab],[3] G. Eigen,[4] B. Stugu,[4] L. Sun,[4] G. S. Abrams,[5] M. Battaglia,[5] D. N. Brown,[5] R. N. Cahn,[5] R. G. Jacobsen,[5] L. T. Kerth,[5] Yu. G. Kolomensky,[5] G. Kukartsev,[5] G. Lynch,[5] I. L. Osipenkov,[5] M. T. Ronan,[5,*] K. Tackmann,[5] T. Tanabe,[5] C. M. Hawkes,[6] N. Soni,[6] A. T. Watson,[6] H. Koch,[7] T. Schroeder,[7] D. Walker,[8] D. J. Asgeirsson,[9] T. Cuhadar-Donszelmann,[9] B. G. Fulsom,[9] C. Hearty,[9] T. S. Mattison,[9] J. A. McKenna,[9] M. Barrett,[10] A. Khan,[10] L. Teodorescu,[10] V. E. Blinov,[11] A. D. Bukin,[11] A. R. Buzykaev,[11] V. P. Druzhinin,[11] V. B. Golubev,[11] A. P. Onuchin,[11] S. I. Serednyakov,[11] Yu. I. Skovpen,[11] E. P. Solodov,[11] K. Yu. Todyshev,[11] M. Bondioli,[12] S. Curry,[12] I. Eschrich,[12] D. Kirkby,[12] A. J. Lankford,[12] P. Lund,[12] M. Mandelkern,[12] E. C. Martin,[12] D. P. Stoker,[12] S. Abachi,[13] C. Buchanan,[13] J. W. Gary,[14] F. Liu,[14] O. Long,[14] B. C. Shen,[14,*] G. M. Vitug,[14] Z. Yasin,[14] L. Zhang,[14] V. Sharma,[15] C. Campagnari,[16] T. M. Hong,[16] D. Kovalskyi,[16] M. A. Mazur,[16] J. D. Richman,[16] T. W. Beck,[17] A. M. Eisner,[17] C. J. Flacco,[17] C. A. Heusch,[17] J. Kroseberg,[17] W. S. Lockman,[17] T. Schalk,[17] B. A. Schumm,[17] A. Seiden,[17] L. Wang,[17] M. G. Wilson,[17] L. O. Winstrom,[17] C. H. Cheng,[18] D. A. Doll,[18] B. Echenard,[18] F. Fang,[18] D. G. Hitlin,[18] I. Narsky,[18] T. Piatenko,[18] F. C. Porter,[18] R. Andreassen,[19] G. Mancinelli,[19] B. T. Meadows,[19] K. Mishra,[19] M. D. Sokoloff,[19] F. Blanc,[20] P. C. Bloom,[20] W. T. Ford,[20] A. Gaz,[20] J. F. Hirschauer,[20] A. Kreisel,[20] M. Nagel,[20] U. Nauenberg,[20] J. G. Smith,[20] K. A. Ulmer,[20] S. R. Wagner,[20] R. Ayad,[21,†] A. Soffer,[21,‡] W. H. Toki,[21] R. J. Wilson,[21] D. D. Altenburg,[22] E. Feltresi,[22] A. Hauke,[22] H. Jasper,[22] M. Karbach,[22] J. Merkel,[22] A. Petzold,[22] B. Spaan,[22] K. Wacker,[22] M. J. Kobel,[23] W. F. Mader,[23] R. Nogowski,[23] K. R. Schubert,[23] R. Schwierz,[23] J. E. Sundermann,[23] A. Volk,[23] D. Bernard,[24] G. R. Bonneaud,[24] E. Latour,[24] Ch. Thiebaux,[24] M. Verderi,[24] P. J. Clark,[25] W. Gradl,[25] S. Playfer,[25] J. E. Watson,[25] M. Andreotti[ab],[26] D. Bettoni[a],[26] C. Bozzi[a],[26] R. Calabrese[ab],[26] A. Cecchi[ab],[26] G. Cibinetto[ab],[26] P. Franchini[ab],[26] E. Luppi[ab],[26] M. Negrini[ab],[26] A. Petrella[ab],[26] L. Piemontese[a],[26] V. Santoro[ab],[26] R. Baldini-Ferroli,[27] A. Calcaterra,[27] R. de Sangro,[27] G. Finocchiaro,[27] S. Pacetti,[27] P. Patteri,[27] I. M. Peruzzi,[27,§] M. Piccolo,[27] M. Rama,[27] A. Zallo,[27] A. Buzzo[a],[28] R. Contri[ab],[28] M. Lo Vetere[ab],[28] M. M. Macri[a],[28] M. R. Monge[ab],[28] S. Passaggio[a],[28] C. Patrignani[ab],[28] E. Robutti[a],[28] A. Santroni[ab],[28] S. Tosi[ab],[28] K. S. Chaisanguanthum,[29] M. Morii,[29] R. S. Dubitzky,[30] J. Marks,[30] S. Schenk,[30] U. Uwer,[30] V. Klose,[31] H. M. Lacker,[31] G. De Nardo[ab],[32] L. Lista[a],[32] D. Monorchio[ab],[32] G. Onorato[ab],[32] C. Sciacca[ab],[32] D. J. Bard,[33] P. D. Dauncey,[33] J. A. Nash,[33] W. Panduro Vazquez,[33] M. Tibbetts,[33] P. K. Behera,[34] X. Chai,[34] M. J. Charles,[34] U. Mallik,[34] J. Cochran,[35] H. B. Crawley,[35] L. Dong,[35] W. T. Meyer,[35] S. Prell,[35] E. I. Rosenberg,[35] A. E. Rubin,[35] Y. Y. Gao,[36] A. V. Gritsan,[36] Z. J. Guo,[36] C. K. Lae,[36] A. G. Denig,[37] M. Fritsch,[37] G. Schott,[37] N. Arnaud,[38] J. Béquilleux,[38] A. D'Orazio,[38] M. Davier,[38] J. Firmino da Costa,[38] G. Grosdidier,[38] A. Höcker,[38] V. Lepeltier,[38] F. Le Diberder,[38] A. M. Lutz,[38] S. Pruvot,[38] P. Roudeau,[38] M. H. Schune,[38] J. Serrano,[38] V. Sordini,[38,¶] A. Stocchi,[38] G. Wormser,[38] D. J. Lange,[39] D. M. Wright,[39] I. Bingham,[40] J. P. Burke,[40] C. A. Chavez,[40] J. R. Fry,[40] E. Gabathuler,[40] R. Gamet,[40] D. E. Hutchcroft,[40] D. J. Payne,[40] C. Touramanis,[40] A. J. Bevan,[41] K. A. George,[41] F. Di Lodovico,[41] R. Sacco,[41] M. Sigamani,[41] G. Cowan,[42] H. U. Flaecher,[42] D. A. Hopkins,[42] S. Paramesvaran,[42] F. Salvatore,[42] A. C. Wren,[42] D. N. Brown,[43] C. L. Davis,[43] K. E. Alwyn,[44] N. R. Barlow,[44] R. J. Barlow,[44] Y. M. Chia,[44] C. L. Edgar,[44] G. D. Lafferty,[44] T. J. West,[44] J. I. Yi,[44] J. Anderson,[45] C. Chen,[45] A. Jawahery,[45] D. A. Roberts,[45] G. Simi,[45] J. M. Tuggle,[45] C. Dallapiccola,[46] S. S. Hertzbach,[46] X. Li,[46] E. Salvati,[46] S. Saremi,[46] R. Cowan,[47] D. Dujmic,[47] P. H. Fisher,[47] K. Koeneke,[47] G. Sciolla,[47] M. Spitznagel,[47] F. Taylor,[47] R. K. Yamamoto,[47] M. Zhao,[47] S. E. Mclachlin,[48,*] P. M. Patel,[48] S. H. Robertson,[48] A. Lazzaro[ab],[49] V. Lombardo[a],[49] F. Palombo[ab],[49] J. M. Bauer,[50] L. Cremaldi,[50] V. Eschenburg,[50] R. Godang,[50,**] R. Kroeger,[50] D. A. Sanders,[50] D. J. Summers,[50] H. W. Zhao,[50] M. Simard,[51] P. Taras,[51] F. B. Viaud,[51] H. Nicholson,[52] M. A. Baak,[53] G. Raven,[53] H. L. Snoek,[53] C. P. Jessop,[54] K. J. Knoepfel,[54] J. M. LoSecco,[54] W. F. Wang,[54] G. Benelli,[55] L. A. Corwin,[55] K. Honscheid,[55]

Published in the Physical Review D

Work supported in part by US Department of Energy contract DE-AC02-76SF00515

H. Kagan,[55] R. Kass,[55] J. P. Morris,[55] A. M. Rahimi,[55] J. J. Regensburger,[55] S. J. Sekula,[55] Q. K. Wong,[55] N. L. Blount,[56] J. Brau,[56] R. Frey,[56] O. Igonkina,[56] J. A. Kolb,[56] M. Lu,[56] R. Rahmat,[56] N. B. Sinev,[56] D. Strom,[56] J. Strube,[56] E. Torrence,[56] G. Castelli[ab],[57] N. Gagliardi[ab],[57] M. Margoni[ab],[57] M. Morandin[a],[57] M. Posocco[a],[57] M. Rotondo[a],[57] F. Simonetto[ab],[57] R. Stroili[ab],[57] C. Voci[ab],[57] P. del Amo Sanchez,[58] E. Ben-Haim,[58] H. Briand,[58] G. Calderini,[58] J. Chauveau,[58] P. David,[58] L. Del Buono,[58] O. Hamon,[58] Ph. Leruste,[58] J. Ocariz,[58] A. Perez,[58] J. Prendki,[58] L. Gladney,[59] M. Biasini[ab],[60] R. Covarelli[ab],[60] E. Manoni[ab],[60] C. Angelini[ab],[61] G. Batignani[ab],[61] S. Bettarini[ab],[61] M. Carpinelli[ab],[61,††] A. Cervelli[ab],[61] F. Forti[ab],[61] M. A. Giorgi[ab],[61] A. Lusiani[ac],[61] G. Marchiori[ab],[61] M. Morganti[ab],[61] N. Neri[ab],[61] E. Paoloni[ab],[61] G. Rizzo[ab],[61] J. J. Walsh[a],[61] J. Biesiada,[62] D. Lopes Pegna,[62] C. Lu,[62] J. Olsen,[62] A. J. S. Smith,[62] A. V. Telnov,[62] F. Anulli[a],[63] E. Baracchini[ab],[63] G. Cavoto[a],[63] D. del Re[ab],[63] E. Di Marco[ab],[63] R. Faccini[ab],[63] F. Ferrarotto[a],[63] F. Ferroni[ab],[63] M. Gaspero[ab],[63] P. D. Jackson[a],[63] L. Li Gioi[a],[63] M. A. Mazzoni[a],[63] S. Morganti[a],[63] G. Piredda[a],[63] F. Polci[ab],[63] F. Renga[ab],[63] C. Voena[a],[63] M. Ebert,[64] T. Hartmann,[64] H. Schröder,[64] R. Waldi,[64] T. Adye,[65] B. Franek,[65] E. O. Olaiya,[65] W. Roethel,[65] F. F. Wilson,[65] S. Emery,[66] M. Escalier,[66] L. Esteve,[66] A. Gaidot,[66] S. F. Ganzhur,[66] G. Hamel de Monchenault,[66] W. Kozanecki,[66] G. Vasseur,[66] Ch. Yèche,[66] M. Zito,[66] X. R. Chen,[67] H. Liu,[67] W. Park,[67] M. V. Purohit,[67] R. M. White,[67] J. R. Wilson,[67] M. T. Allen,[68] D. Aston,[68] R. Bartoldus,[68] P. Bechtle,[68] J. F. Benitez,[68] R. Cenci,[68] J. P. Coleman,[68] M. R. Convery,[68] J. C. Dingfelder,[68] J. Dorfan,[68] G. P. Dubois-Felsmann,[68] W. Dunwoodie,[68] R. C. Field,[68] A. M. Gabareen,[68] S. J. Gowdy,[68] M. T. Graham,[68] P. Grenier,[68] C. Hast,[68] W. R. Innes,[68] J. Kaminski,[68] M. H. Kelsey,[68] H. Kim,[68] P. Kim,[68] M. L. Kocian,[68] D. W. G. S. Leith,[68] S. Li,[68] B. Lindquist,[68] S. Luitz,[68] V. Luth,[68] H. L. Lynch,[68] D. B. MacFarlane,[68] H. Marsiske,[68] R. Messner,[68] D. R. Muller,[68] H. Neal,[68] S. Nelson,[68] C. P. O'Grady,[68] I. Ofte,[68] A. Perazzo,[68] M. Perl,[68] B. N. Ratcliff,[68] A. Roodman,[68] A. A. Salnikov,[68] R. H. Schindler,[68] J. Schwiening,[68] A. Snyder,[68] D. Su,[68] M. K. Sullivan,[68] K. Suzuki,[68] S. K. Swain,[68] J. M. Thompson,[68] J. Va'vra,[68] A. P. Wagner,[68] M. Weaver,[68] C. A. West,[68] W. J. Wisniewski,[68] M. Wittgen,[68] D. H. Wright,[68] H. W. Wulsin,[68] A. K. Yarritu,[68] K. Yi,[68] C. C. Young,[68] V. Ziegler,[68] P. R. Burchat,[69] A. J. Edwards,[69] S. A. Majewski,[69] T. S. Miyashita,[69] B. A. Petersen,[69] L. Wilden,[69] S. Ahmed,[70] M. S. Alam,[70] R. Bula,[70] J. A. Ernst,[70] B. Pan,[70] M. A. Saeed,[70] S. B. Zain,[70] S. M. Spanier,[71] B. J. Wogsland,[71] R. Eckmann,[72] J. L. Ritchie,[72] A. M. Ruland,[72] C. J. Schilling,[72] R. F. Schwitters,[72] B. W. Drummond,[73] J. M. Izen,[73] X. C. Lou,[73] F. Bianchi[ab],[74] D. Gamba[ab],[74] M. Pelliccioni[ab],[74] M. Bomben[ab],[75] L. Bosisio[ab],[75] C. Cartaro[ab],[75] G. Della Ricca[ab],[75] L. Lanceri[ab],[75] L. Vitale[ab],[75] V. Azzolini,[76] N. Lopez-March,[76] F. Martinez-Vidal,[76] D. A. Milanes,[76] A. Oyanguren,[76] J. Albert,[77] Sw. Banerjee,[77] B. Bhuyan,[77] H. H. F. Choi,[77] K. Hamano,[77] R. Kowalewski,[77] M. J. Lewczuk,[77] I. M. Nugent,[77] J. M. Roney,[77] R. J. Sobie,[77] T. J. Gershon,[78] P. F. Harrison,[78] J. Ilic,[78] T. E. Latham,[78] G. B. Mohanty,[78] H. R. Band,[79] X. Chen,[79] S. Dasu,[79] K. T. Flood,[79] Y. Pan,[79] M. Pierini,[79] R. Prepost,[79] C. O. Vuosalo,[79] and S. L. Wu[79]

(The *BABAR* Collaboration)

[1] *Laboratoire de Physique des Particules, IN2P3/CNRS et Université de Savoie, F-74941 Annecy-Le-Vieux, France*
[2] *Universitat de Barcelona, Facultat de Fisica, Departament ECM, E-08028 Barcelona, Spain*
[3] *INFN Sezione di Bari[a]; Dipartmento di Fisica, Università di Bari[b], I-70126 Bari, Italy*
[4] *University of Bergen, Institute of Physics, N-5007 Bergen, Norway*
[5] *Lawrence Berkeley National Laboratory and University of California, Berkeley, California 94720, USA*
[6] *University of Birmingham, Birmingham, B15 2TT, United Kingdom*
[7] *Ruhr Universität Bochum, Institut für Experimentalphysik 1, D-44780 Bochum, Germany*
[8] *University of Bristol, Bristol BS8 1TL, United Kingdom*
[9] *University of British Columbia, Vancouver, British Columbia, Canada V6T 1Z1*
[10] *Brunel University, Uxbridge, Middlesex UB8 3PH, United Kingdom*
[11] *Budker Institute of Nuclear Physics, Novosibirsk 630090, Russia*
[12] *University of California at Irvine, Irvine, California 92697, USA*
[13] *University of California at Los Angeles, Los Angeles, California 90024, USA*
[14] *University of California at Riverside, Riverside, California 92521, USA*
[15] *University of California at San Diego, La Jolla, California 92093, USA*
[16] *University of California at Santa Barbara, Santa Barbara, California 93106, USA*
[17] *University of California at Santa Cruz, Institute for Particle Physics, Santa Cruz, California 95064, USA*
[18] *California Institute of Technology, Pasadena, California 91125, USA*
[19] *University of Cincinnati, Cincinnati, Ohio 45221, USA*
[20] *University of Colorado, Boulder, Colorado 80309, USA*
[21] *Colorado State University, Fort Collins, Colorado 80523, USA*
[22] *Technische Universität Dortmund, Fakultät Physik, D-44221 Dortmund, Germany*

[23] Technische Universität Dresden, Institut für Kern- und Teilchenphysik, D-01062 Dresden, Germany
[24] Laboratoire Leprince-Ringuet, CNRS/IN2P3, Ecole Polytechnique, F-91128 Palaiseau, France
[25] University of Edinburgh, Edinburgh EH9 3JZ, United Kingdom
[26] INFN Sezione di Ferrara[a]; Dipartimento di Fisica, Università di Ferrara[b], I-44100 Ferrara, Italy
[27] INFN Laboratori Nazionali di Frascati, I-00044 Frascati, Italy
[28] INFN Sezione di Genova[a]; Dipartimento di Fisica, Università di Genova[b], I-16146 Genova, Italy
[29] Harvard University, Cambridge, Massachusetts 02138, USA
[30] Universität Heidelberg, Physikalisches Institut, Philosophenweg 12, D-69120 Heidelberg, Germany
[31] Humboldt-Universität zu Berlin, Institut für Physik, Newtonstr. 15, D-12489 Berlin, Germany
[32] INFN Sezione di Napoli[a]; Dipartimento di Scienze Fisiche,
Università di Napoli Federico II[b], I-80126 Napoli, Italy
[33] Imperial College London, London, SW7 2AZ, United Kingdom
[34] University of Iowa, Iowa City, Iowa 52242, USA
[35] Iowa State University, Ames, Iowa 50011-3160, USA
[36] Johns Hopkins University, Baltimore, Maryland 21218, USA
[37] Universität Karlsruhe, Institut für Experimentelle Kernphysik, D-76021 Karlsruhe, Germany
[38] Laboratoire de l'Accélérateur Linéaire, IN2P3/CNRS et Université Paris-Sud 11,
Centre Scientifique d'Orsay, B. P. 34, F-91898 ORSAY Cedex, France
[39] Lawrence Livermore National Laboratory, Livermore, California 94550, USA
[40] University of Liverpool, Liverpool L69 7ZE, United Kingdom
[41] Queen Mary, University of London, E1 4NS, United Kingdom
[42] University of London, Royal Holloway and Bedford New College, Egham, Surrey TW20 0EX, United Kingdom
[43] University of Louisville, Louisville, Kentucky 40292, USA
[44] University of Manchester, Manchester M13 9PL, United Kingdom
[45] University of Maryland, College Park, Maryland 20742, USA
[46] University of Massachusetts, Amherst, Massachusetts 01003, USA
[47] Massachusetts Institute of Technology, Laboratory for Nuclear Science, Cambridge, Massachusetts 02139, USA
[48] McGill University, Montréal, Québec, Canada H3A 2T8
[49] INFN Sezione di Milano[a]; Dipartimento di Fisica, Università di Milano[b], I-20133 Milano, Italy
[50] University of Mississippi, University, Mississippi 38677, USA
[51] Université de Montréal, Physique des Particules, Montréal, Québec, Canada H3C 3J7
[52] Mount Holyoke College, South Hadley, Massachusetts 01075, USA
[53] NIKHEF, National Institute for Nuclear Physics and High Energy Physics, NL-1009 DB Amsterdam, The Netherlands
[54] University of Notre Dame, Notre Dame, Indiana 46556, USA
[55] Ohio State University, Columbus, Ohio 43210, USA
[56] University of Oregon, Eugene, Oregon 97403, USA
[57] INFN Sezione di Padova[a]; Dipartimento di Fisica, Università di Padova[b], I-35131 Padova, Italy
[58] Laboratoire de Physique Nucléaire et de Hautes Energies,
IN2P3/CNRS, Université Pierre et Marie Curie-Paris6,
Université Denis Diderot-Paris7, F-75252 Paris, France
[59] University of Pennsylvania, Philadelphia, Pennsylvania 19104, USA
[60] INFN Sezione di Perugia[a]; Dipartimento di Fisica, Università di Perugia[b], I-06100 Perugia, Italy
[61] INFN Sezione di Pisa[a]; Dipartimento di Fisica,
Università di Pisa[b]; Scuola Normale Superiore di Pisa[c], I-56127 Pisa, Italy
[62] Princeton University, Princeton, New Jersey 08544, USA
[63] INFN Sezione di Roma[a]; Dipartimento di Fisica,
Università di Roma La Sapienza[b], I-00185 Roma, Italy
[64] Universität Rostock, D-18051 Rostock, Germany
[65] Rutherford Appleton Laboratory, Chilton, Didcot, Oxon, OX11 0QX, United Kingdom
[66] DSM/Dapnia, CEA/Saclay, F-91191 Gif-sur-Yvette, France
[67] University of South Carolina, Columbia, South Carolina 29208, USA
[68] Stanford Linear Accelerator Center, Stanford, California 94309, USA
[69] Stanford University, Stanford, California 94305-4060, USA
[70] State University of New York, Albany, New York 12222, USA
[71] University of Tennessee, Knoxville, Tennessee 37996, USA
[72] University of Texas at Austin, Austin, Texas 78712, USA
[73] University of Texas at Dallas, Richardson, Texas 75083, USA
[74] INFN Sezione di Torino[a]; Dipartimento di Fisica Sperimentale, Università di Torino[b], I-10125 Torino, Italy
[75] INFN Sezione di Trieste[a]; Dipartimento di Fisica, Università di Trieste[b], I-34127 Trieste, Italy
[76] IFIC, Universitat de Valencia-CSIC, E-46071 Valencia, Spain
[77] University of Victoria, Victoria, British Columbia, Canada V8W 3P6
[78] Department of Physics, University of Warwick, Coventry CV4 7AL, United Kingdom
[79] University of Wisconsin, Madison, Wisconsin 53706, USA

We present an investigation of the decays $\overline{B}^0 \to \Lambda_c^+ \overline{p}$ and $B^- \to \Lambda_c^+ \overline{p}\pi^-$ based on 383×10^6 $\Upsilon(4S) \to B\overline{B}$ decays recorded with the *BABAR* detector. We measure the branching fractions of these decays; their ratio is $\mathcal{B}(B^- \to \Lambda_c^+ \overline{p}\pi^-)/\mathcal{B}(\overline{B}^0 \to \Lambda_c^+ \overline{p}) = 15.4 \pm 1.8 \pm 0.3$. The $B^- \to \Lambda_c^+ \overline{p}\pi^-$ process exhibits an enhancement at the $\Lambda_c^+ \overline{p}$ threshold and is a laboratory for searches for excited charm baryon states. We observe the resonant decays $B^- \to \Sigma_c(2455)^0 \overline{p}$ and $B^- \to \Sigma_c(2800)^0 \overline{p}$ but see no evidence for $B^- \to \Sigma_c(2520)^0 \overline{p}$. This is the first observation of the decay $B^- \to \Sigma_c(2800)^0 \overline{p}$; however, the mass of the observed excited Σ_c^0 state is $(2846 \pm 8 \pm 10)\,\mathrm{MeV}/c^2$, which is somewhat inconsistent with previous measurements. Finally, we examine the angular distribution of the $B^- \to \Sigma_c(2455)^0 \overline{p}$ decays and measure the spin of the $\Sigma_c(2455)^0$ baryon to be 1/2, as predicted by the quark model.

PACS numbers: 13.25.Hw, 13.60.Rj, 14.20.Lq

INTRODUCTION

Baryonic decays of B mesons, which contain a heavy bottom quark and a light up or down quark, provide a laboratory for a range of particle physics investigations: trends in decay rates and baryon production mechanisms; searches for exotic states such as pentaquarks and glueballs [1, 2]; searches for excited baryon resonances; examination of the angular distributions of B-meson decay products to determine baryon spins; and measurements of radiative baryonic B decays that could be sensitive to new physics through flavor-changing neutral currents [3, 4]. The latter measurements rely on improving our theoretical understanding of baryonic B decays in general [5, 6].

The inclusive branching fraction for baryonic B decays is $(6.8 \pm 0.6)\%$ [7], and many exclusive baryonic B decay modes have been observed [8]. If we order the measured decays by Q-value:

$$Q = m_B - \sum_f m_f, \tag{1}$$

where m_f is the mass of each daughter in the final state of the B decay, we find that for each type of baryonic B decay, the branching fractions decrease as the Q-value increases. The smallest measured branching fraction is of the order 10^{-6}, which also corresponds to our experimental sensitivity for measuring these branching fractions. Potentially interesting B-meson decays such as $B \to p\overline{p}$, $B \to \Lambda\overline{\Lambda}$, and $B \to \Lambda_c^+ \overline{\Lambda}_c^-$ have not yet been seen.

Theoretical approaches to calculating baryonic B decays include pole models [9, 10], diquark models [11], and QCD sum rules [12, 13]. Recently, theoretical calculations have focused on pole models, where the B decay proceeds through an intermediate b-flavored baryon state, which then decays weakly into one of the final state baryons [14, 15]. However, it is not clear that the pole model is reliable for baryon poles, and the predictions given in the literature vary significantly. Perhaps the most satisfying theoretical interpretation of baryonic B decay rates is the qualitative one proposed by Hou and Soni in 2001 [16], who argue that B decays are favored if the baryon and antibaryon in the final-state configuration are close together in phase space. A consequence is that decay rates to two-body baryon-antibaryon final states are suppressed relative to rates of three-body final states containing the same baryon-antibaryon system plus an additional meson. In the three-body case, the baryon and antibaryon can be in the favored configuration—close together in phase space—rather than back-to-back as in the two-body case.

In this paper, we investigate the decays $\overline{B}^0 \to \Lambda_c^+ \overline{p}$ and $B^- \to \Lambda_c^+ \overline{p}\pi^-$ [17]. We investigate baryon production in B decays by comparing the two-body ($\overline{B}^0 \to \Lambda_c^+ \overline{p}$) and three-body ($B^- \to \Lambda_c^+ \overline{p}\pi^-$) decay rates directly. The dynamics of the baryon-antibaryon ($\Lambda_c^+ \overline{p}$) system in the three-body decay provide insight into baryon production mechanisms. Additionally, the $B^- \to \Lambda_c^+ \overline{p}\pi^-$ system is a laboratory for studying excited baryon states and is used to measure the spin of the $\Sigma_c(2455)^0$. This is the first measurement of the spin of this state.

BABAR DETECTOR AND DATA SAMPLE

The measurements presented in this paper are based on 383×10^6 $\Upsilon(4S) \to B\overline{B}$ decays recorded with the *BABAR* detector [18] at the PEP-II e^+e^- asymmetric-energy B Factory at the Stanford Linear Accelerator Center. At the interaction point, 9- GeV electrons collide with 3.1- GeV positrons at the $\Upsilon(4S)$ resonance with a center-of-mass energy of $10.58\,\mathrm{GeV}/c^2$.

Charged particle trajectories are measured by a five-layer silicon vertex tracker (SVT) and a 40-layer drift chamber (DCH) immersed in a 1.5-T axial magnetic field. Charged particle identification is provided by ionization energy ($\mathrm{d}E/\mathrm{d}x$) measurements in the SVT and DCH along with Cherenkov radiation detection by an inter-

*Deceased
†Now at Temple University, Philadelphia, PA 19122, USA
‡Now at Tel Aviv University, Tel Aviv, 69978, Israel
§Also with Università di Perugia, Dipartimento di Fisica, Perugia, Italy
¶Also with Università di Roma La Sapienza, I-00185 Roma, Italy
**Now at University of South Alabama, Mobile, AL 36688, USA
††Also with Università di Sassari, Sassari, Italy

nally reflecting ring-imaging detector (DRC).

Exclusive B-meson decays are simulated with the Monte Carlo (MC) event generator `EvtGen` [19]. Background continuum MC samples ($e^+e^- \to q\overline{q}$, where $q = u, d, s, c$) are simulated using `Jetset7.4` [20] to model generic hadronization processes. Background MC samples of $e^+e^- \to B^+B^-$ and $B^0\overline{B}^0$ are based on simulations of many exclusive B decays (also using `EvtGen`). The large samples of simulated events are generated and propagated through a detailed detector simulation using the `GEANT4` simulation package [21].

CANDIDATE SELECTION

We select candidates that are kinematically consistent with $\overline{B}^0 \to \Lambda_c^+\overline{p}$ and $B^- \to \Lambda_c^+\overline{p}\pi^-$. For the decay mode $\overline{B}^0 \to \Lambda_c^+\overline{p}$, we reconstruct Λ_c^+ candidates in the $pK^-\pi^+$, pK_S^0, $pK_S^0\pi^+\pi^-$, and $\Lambda\pi^+$ decay modes, requiring the invariant mass of each Λ_c^+ candidate to be within $10\,\mathrm{MeV}/c^2$ of the world average value [8]. For $B^- \to \Lambda_c^+\overline{p}\pi^-$, we also reconstruct Λ_c^+ candidates in the $\Lambda\pi^+\pi^-\pi^+$ decay mode, and require all of the Λ_c^+ candidates to have an invariant mass within $12\,\mathrm{MeV}/c^2$ of the world average value.

The p, K, and π candidates must be well-reconstructed in the DCH and are identified with likelihood-based particle selectors using information from the SVT, DCH, and DRC.

The K_S^0 candidates are reconstructed from two oppositely charged pion candidates that come from a common vertex; Λ candidates are formed by combining a proton candidate with an oppositely charged pion candidate that comes from a common vertex. The invariant mass of each K_S^0 and Λ candidate must be within $10\,\mathrm{MeV}/c^2$ of the world average value [8] and the flight significance (defined as the flight distance from the Λ_c^+ vertex in the $x-y$ plane divided by the measurement uncertainty) must be greater than 2. The mass of each K_S^0 and Λ candidate is then constrained to the world average value [8].

A mass constraint is applied to all of the Λ_c^+ candidates, and all Λ_c^+ daughter tracks must come from a common vertex. The Λ_c^+ candidates are then combined with an antiproton to form a $\overline{B}^0 \to \Lambda_c^+\overline{p}$ candidate, or with an antiproton and a pion to form a $B^- \to \Lambda_c^+\overline{p}\pi^-$ candidate. The daughters of each B candidate must come from a common vertex, and the candidate with the largest χ^2 probability in each event is selected.

Additional background suppression is provided by information about the topology of the events. A Fisher discriminant [22] is constructed based on the absolute value of the cosine of the angle of the B candidate momentum vector with respect to the beam axis in the e^+e^- center-of-mass (CM) frame, the absolute value of the cosine of the angle between the B candidate thrust axis [23] and the thrust axis of the rest of the event in the e^+e^- CM frame, and the moments L_0 and L_2. The quantity L_j is defined as $\sum_i p_i\,|\cos\theta_i|^j$, where θ_i is the angle with respect to the B candidate thrust axis of the ith charged particle or neutral cluster in the rest of the event and p_i is its momentum. The optimal maximum value of the Fisher discriminant is chosen separately for each Λ_c^+ and B decay mode.

Kinematic properties of B-meson pair production at the $\Upsilon(4S)$ provide further background discrimination. We define a pair of observables, m_m and m_r, that are uncorrelated and exploit these constraints:

$$m_m = \sqrt{\left(q_{e^+e^-} - \hat{q}_{\Lambda_c^+\overline{p}(\pi^-)}\right)^2} \quad \text{and}$$
$$m_r = \sqrt{\left(q_{\Lambda_c^+\overline{p}(\pi^-)}\right)^2} - m_B. \qquad (2)$$

The variable m_m is based on the apparent recoil mass of the unreconstructed B meson in the event, where $q_{e^+e^-}$ is the four-momentum of the e^+e^- system and $\hat{q}_{\Lambda_c^+\overline{p}(\pi^-)}$ is the four-momentum of the reconstructed B candidate after applying a mass constraint. The variable m_r is the difference between the unconstrained mass of the reconstructed B candidate and m_B, the world average value of the mass of the B meson [8]. Signal events peak at m_B in m_m and 0 in m_r. This set of variables was first used in [24] and is chosen as an uncorrelated alternative to $\Delta E = E_B^* - \frac{1}{2}\sqrt{s}$ and the energy-substituted mass $m_{\rm ES} = \sqrt{\frac{1}{4}s - p_B^{*2}}$ (where $s = q^2_{e^+e^-}$ and the asterisk denotes the e^+e^- rest frame), which exhibit a $\sim 30\%$ correlation for $B^- \to \Lambda_c^+\overline{p}\pi^-$.

The event selection criteria are optimized based on studies of sideband data (in the region $0.10 < m_r < 0.20\,\mathrm{GeV}/c^2$) and simulated signal MC samples. The data in a signal region (approximately $\pm 2\sigma$ wide in m_m and m_r) were blinded until the selection criteria were determined and the signal extraction procedure was specified and validated. B candidates that satisfy $m_m > 5.121\,\mathrm{GeV}/c^2$ and $|m_r| < 0.10\,\mathrm{GeV}/c^2$ are used in the maximum likelihood fit.

BACKGROUNDS

The primary source of background for $\overline{B}^0 \to \Lambda_c^+\overline{p}$ candidates is continuum $e^+e^- \to q\overline{q}$ events. Backgrounds due to decays such as $B^- \to \Lambda_c^+\overline{p}\pi^-$, $\overline{B}^0 \to \Lambda_c^+\overline{p}\pi^0$, and $B^- \to \Sigma_c^0\overline{p}, \Sigma_c^0 \to \Lambda_c^+\pi^-$ are rejected by the criterion $|m_r| < 0.10\,\mathrm{GeV}/c^2$.

Approximately equal amounts of continuum $e^+e^- \to q\overline{q}$ and $e^+e^- \to B\overline{B}$ events make up the background for $B^- \to \Lambda_c^+\overline{p}\pi^-$ events. Again, the requirement $|m_r| < 0.10\,\mathrm{GeV}/c^2$ rejects most of the contributions from such decays as $\overline{B}^0 \to \Lambda_c^+\overline{p}\pi^+\pi^-$ and $B^- \to \Lambda_c^+\overline{p}\pi^-\pi^0$. Approximately 1% of the background in the fit region is due to these four-body events, but they do not peak in m_m and m_r. A small peaking background is present

from $\overline{B}^0 \to \Sigma_c^+ \overline{p}, \Sigma_c^+ \to \Lambda_c^+ \pi^0$ events, especially when the π^0 has low momentum. Based on a branching fraction measurement of the isospin partner decay $\mathcal{B}(B^- \to \Sigma_c(2455)^0 \overline{p}) = (3.7 \pm 0.7 \pm 0.4 \pm 1.0) \times 10^{-5}$ [25], where the uncertainties are statistical, systematic, and the uncertainty due to $\mathcal{B}(\Lambda_c^+ \to pK^-\pi^+)$, respectively, we expect 11.5 ± 2.5 peaking background events in the signal region for $B^- \to \Lambda_c^+ \overline{p}\pi^-$, $\Lambda_c^+ \to pK^-\pi^+$. A correction is applied and a systematic uncertainty is assigned to compensate for these events.

DETECTION EFFICIENCY

The detection efficiencies for $\overline{B}^0 \to \Lambda_c^+ \overline{p}$ and $B^- \to \Lambda_c^+ \overline{p}\pi^-$ signal events are determined from signal MC samples with 175,000 to over 1,600,000 events in each sample, depending on the Λ_c^+ decay mode. To account for inaccuracies in the simulation of the detector, each MC event is assigned a weight based on each daughter particle's momentum and angle. These weights are determined from studies comparing large pure samples of protons, kaons, and pions in MC samples and data. Small corrections $(0.4 - 1.6\%)$ are also applied to account for tracking inefficiencies due to the displaced K_S^0 and Λ vertices. These corrections depend on the K_S^0 and Λ daughter trajectories' transverse momentum and angle, and the distance between the beam spot and the displaced vertex.

The detection efficiency (ε_l) for $\overline{B}^0 \to \Lambda_c^+ \overline{p}$ signal events in each Λ_c^+ decay mode (l) is determined from the number of signal events extracted from an extended unbinned maximum likelihood fit to signal MC events. These events pass the same selection criteria as applied to data. The fit is performed in two dimensions, m_m and m_r. The probability distribution function (PDF) for the background consists of a threshold function [26] in m_m multiplied by a first-order polynomial in m_r; this is the same as the background PDF used in the fit to the $\overline{B}^0 \to \Lambda_c^+ \overline{p}$ data. The signal PDF consists of a Gaussian in m_m multiplied by a modified asymmetric Gaussian with a tail parameter in m_r. The detection efficiencies in each Λ_c^+ decay mode are summarized in Table I.

The detection efficiency for $B^- \to \Lambda_c^+ \overline{p}\pi^-$ signal events in each Λ_c^+ decay mode varies considerably across the Dalitz plane of the three-body decay. For reference, we quote the average efficiencies in Table I, but we apply a more sophisticated treatment to these events. We parameterize the physical Dalitz region using the variables $\cos\theta_h$ and the $\Lambda_c^+ \pi^-$ invariant mass, $m_{\Lambda_c\pi}$. The helicity angle θ_h is defined as the angle between the π^- and the $\overline{p}$ in the B^- rest frame. The quantity $\cos\theta_h$ can be expressed in terms of Lorentz-invariant products of four-vectors. We divide the kinematic region into reasonably sized bins that are uniform in $\cos\theta_h$ (0.2 units wide) and nonuniform in $m_{\Lambda_c\pi}$ ($60 - 200\,\mathrm{MeV}/c^2$ wide). This choice of variables is more conducive to rectangular bins than the traditional set of Dalitz variables. The $m_{\Lambda_c\pi}$ bins are narrower near the kinematic limits where the efficiency changes more rapidly and are centered on expected resonances. For $B^- \to \Lambda_c^+ \overline{p}\pi^-$, $\Lambda_c^+ \to pK^-\pi^+$ near $\cos\theta_h = 0$, the efficiency varies from approximately 13% at low $m_{\Lambda_c\pi}$, to 16% in the central $m_{\Lambda_c\pi}$ region, to 8% at high $m_{\Lambda_c\pi}$. The efficiency is fairly uniform with respect to $\cos\theta_h$, except at $\cos\theta_h \sim 1$ and low $m_{\Lambda_c\pi}$, where it drops to 7.4%. The other Λ_c^+ decay modes exhibit similar variations in efficiency.

TABLE I: Detection efficiency for $\overline{B}^0 \to \Lambda_c^+ \overline{p}$ signal events, determined from signal Monte Carlo samples and separated by Λ_c^+ decay mode. The numbers correspond to the efficiency for $\overline{B}^0 \to \Lambda_c^+ \overline{p}$ ($B^- \to \Lambda_c^+ \overline{p}\pi^-$), $\Lambda_c^+ \to f_l$, where f_l is a given final state. The efficiencies quoted for the $B^- \to \Lambda_c^+ \overline{p}\pi^-$ decays are averaged across phase space.

	Efficiency for $\Lambda_c^+ \to f_l$	
f_l	$\overline{B}^0 \to \Lambda_c^+ \overline{p}$	$B^- \to \Lambda_c^+ \overline{p}\pi^-$
$pK^-\pi^+$	22.9%	15.4%
pK_S^0	21.6%	14.3%
$pK_S^0\pi^+\pi^-$	9.6%	5.6%
$\Lambda\pi^+$	17.2%	11.6%
$\Lambda\pi^+\pi^-\pi^+$	–	4.0%

SIGNAL EXTRACTION

To extract the number of signal events in data, a two-dimensional (m_m vs. m_r) extended unbinned maximum likelihood fit is performed simultaneously across Λ_c^+ decay modes. $\overline{B}^0 \to \Lambda_c^+ \overline{p}$ candidates and $B^- \to \Lambda_c^+ \overline{p}\pi^-$ candidates are fit separately.

The background PDF for each fit is a threshold function [26] in m_m multiplied by a first-order polynomial in m_r. The shape parameter ($\vec{s}_{bkg}$) of the threshold function is free but is common to all of the Λ_c^+ decay modes. The slope a of the first-order polynomial is allowed to vary independently for each Λ_c^+ decay mode.

The signal PDF is a single Gaussian distribution in m_m multiplied by a single Gaussian distribution in m_r for $\overline{B}^0 \to \Lambda_c^+ \overline{p}$ and multiplied by a double Gaussian distribution in m_r for $B^- \to \Lambda_c^+ \overline{p}\pi^-$. A single Gaussian is sufficient to describe the signal PDF for $\overline{B}^0 \to \Lambda_c^+ \overline{p}$ because of the small number of expected signal events. All of the shape parameters of the signal PDF ($\vec{s}_{sig}$) are free but are shared among the Λ_c^+ decay modes. Separate signal ($N_{sig,l}$) and background ($N_{bkg,l}$) yields are extracted for each Λ_c^+ decay mode l.

The total likelihood is the product of the likelihoods

TABLE II: Signal yields from simultaneous fits (across Λ_c^+ decay modes) to $\overline{B}^0 \to \Lambda_c^+ \overline{p}$ and $B^- \to \Lambda_c^+ \overline{p}\pi^-$ candidates.

	N_{sig}	
Mode	$\overline{B}^0 \to \Lambda_c^+ \overline{p}$	$B^- \to \Lambda_c^+ \overline{p}\pi^-$
$pK^-\pi^+$	90 ± 11	991 ± 45
pK_S^0	10 ± 4	165 ± 15
$pK_S^0\pi^+\pi^-$	14 ± 5	86 ± 14
$\Lambda\pi^+$	3 ± 3	114 ± 13
$\Lambda\pi^+\pi^-\pi^+$	–	88 ± 13

for each Λ_c^+ decay mode:

$$\mathcal{L}_{tot} = \prod_l \mathcal{L}_l \left(\vec{y}_l; N_{sig,l}, N_{bkg,l}, \vec{s}_{sig}, \vec{s}_{bkg}, a_l\right). \quad (3)$$

The symbol $\vec{y}$ represents the variables used in the 2-D fit, $\{m_m, m_r\}$.

The full simultaneous fit is validated using independent samples of signal MC events to simulate signal events and toy MC samples (generated from the background MC sample distribution) to represent background events in the fit region. For both $\overline{B}^0 \to \Lambda_c^+ \overline{p}$ and $B^- \to \Lambda_c^+ \overline{p}\pi^-$, we perform fits to 100 combined MC samples and find that the fit is robust and the results are unbiased.

The results of the 2-D fits to data are shown in projections of m_m and m_r for each Λ_c^+ decay mode. Figure 1 shows the result of the fit to $\overline{B}^0 \to \Lambda_c^+ \overline{p}$ candidates and Fig. 2 shows the result of the fit to $B^- \to \Lambda_c^+ \overline{p}\pi^-$ candidates. The signal yields from the fits are summarized in Table II.

BRANCHING FRACTION MEASUREMENTS

For the three-body mode $B^- \to \Lambda_c^+ \overline{p}\pi^-$, the efficiency variation across the Dalitz plane requires a correction for each signal event in order to extract the branching fraction for this mode. We use the ${}_s\mathcal{P}lot$ method [27] to calculate a weight for each event e based on the 2-D fit to the variables $\vec{y}$. We have $N_s = 2$ species (signal and background) for each Λ_c^+ decay mode and define $f_{j,k}$ as the signal $(j,k=1)$ or background $(j,k=2)$ PDF. The ${}_s\mathcal{P}lot$ weights are calculated as

$${}_s\mathcal{P}_n(\vec{y}_e) = \frac{\sum_{j=1}^{N_s} \mathbf{V}_{nj} f_j(\vec{y}_e)}{\sum_{k=1}^{N_s} N_k f_k(\vec{y}_e)}, \quad (4)$$

where ${}_s\mathcal{P}_n(\vec{y}_e)$ is the ${}_s\mathcal{P}lot$ weight for species n, $\mathbf{V}$ is the covariance matrix for signal and background yields, $f_{j,k}(\vec{y}_e)$ is the value of PDF $f_{j,k}$ for event e, and $\vec{y}_e$ is the m_m and m_r value for event e. The elements of the inverse of the covariance matrix $\mathbf{V}$ are calculated as follows:

$$\mathbf{V}^{-1}_{nj} = \frac{\partial^2(-\ln\mathcal{L})}{\partial N_n \partial N_j} = \sum_{e=1}^{N} \frac{f_n(\vec{y}_e) f_j(\vec{y}_e)}{\left(\sum_{k=1}^{N_s} N_k f_k(\vec{y}_e)\right)^2}, \quad (5)$$

where the sum is over the N candidates. Note that in the calculation of the covariance matrix, the data is refit to the same simultaneous PDF described above, except that all fit parameters other than the yields are fixed to the values from the original fit.

We use these ${}_s\mathcal{P}lot$ weights to generate a signal or background distribution for any quantity that is not correlated with m_m or m_r. The ${}_s\mathcal{P}lot$ formalism is easily extended to incorporate an efficiency correction for each candidate. Each candidate is assigned a weight of $1/\varepsilon$, where the efficiency ε for an event is determined by its location in the $\cos\theta_h$ vs. $m_{\Lambda_c\pi}$ plane.

The branching fraction for $\overline{B}^0 \to \Lambda_c^+ \overline{p}$ for Λ_c^+ decay mode l is calculated as follows:

$$\mathcal{B}(\overline{B}^0 \to \Lambda_c^+ \overline{p})_l = \frac{N_{sig,l}}{N_{B\overline{B}} \times \varepsilon_l \times \mathcal{R}_l \times \mathcal{B}(\Lambda_c^+ \to pK^-\pi^+)}, \quad (6)$$

where $N_{B\overline{B}}$ is the number of $B\overline{B}$ events in the data sample and $\mathcal{R}_l$ is the ratio of Λ_c^+ branching fraction for decay mode l to $\mathcal{B}(\Lambda_c^+ \to pK^-\pi^+)$, taking care to include the $K_S^0 \to \pi^+\pi^-$ and $\Lambda \to p\pi^-$ branching fractions where applicable.

In order to determine the branching fraction for $B^- \to \Lambda_c^+ \overline{p}\pi^-$, we take the product of the ${}_s\mathcal{P}lot$ weight and efficiency weight for each candidate and sum over all of the candidates in the fit region. We simplify the notation by using ${}_sW_i$ to denote the value of the signal ${}_s\mathcal{P}lot$ weight for event i and include a 1% correction for the peaking background due to $\overline{B}^0 \to \Sigma_c^+ \overline{p}, \Sigma_c^+ \to \Lambda_c^+ \pi^0$:

$$\mathcal{B}(B^- \to \Lambda_c^+ \overline{p}\pi^-)_l = \frac{0.99 \times \left(\sum_i \frac{{}_sW_i}{\varepsilon_i}\right)_l}{N_{B\overline{B}} \times \mathcal{R}_l \times \mathcal{B}(\Lambda_c^+ \to pK^-\pi^+)}. \quad (7)$$

The contribution from the peaking background is estimated using the $\Lambda_c^+ \to pK^-\pi^+$ decay mode. Since the overall branching fraction for the peaking background contribution is the same regardless of Λ_c^+ decay mode, it is applied as a proportional correction. The measurements for $\mathcal{B}(\overline{B}^0 \to \Lambda_c^+ \overline{p})$ and $\mathcal{B}(B^- \to \Lambda_c^+ \overline{p}\pi^-)$ for each Λ_c^+ decay mode are summarized in Table III.

The BLUE (Best Linear Unbiased Estimate) technique is used as described in Ref. [28] to combine the *correlated* branching fraction measurements for different Λ_c^+ decay modes. The purpose of the method is to obtain an estimate $\hat{x}$ that is a linear combination of t individual

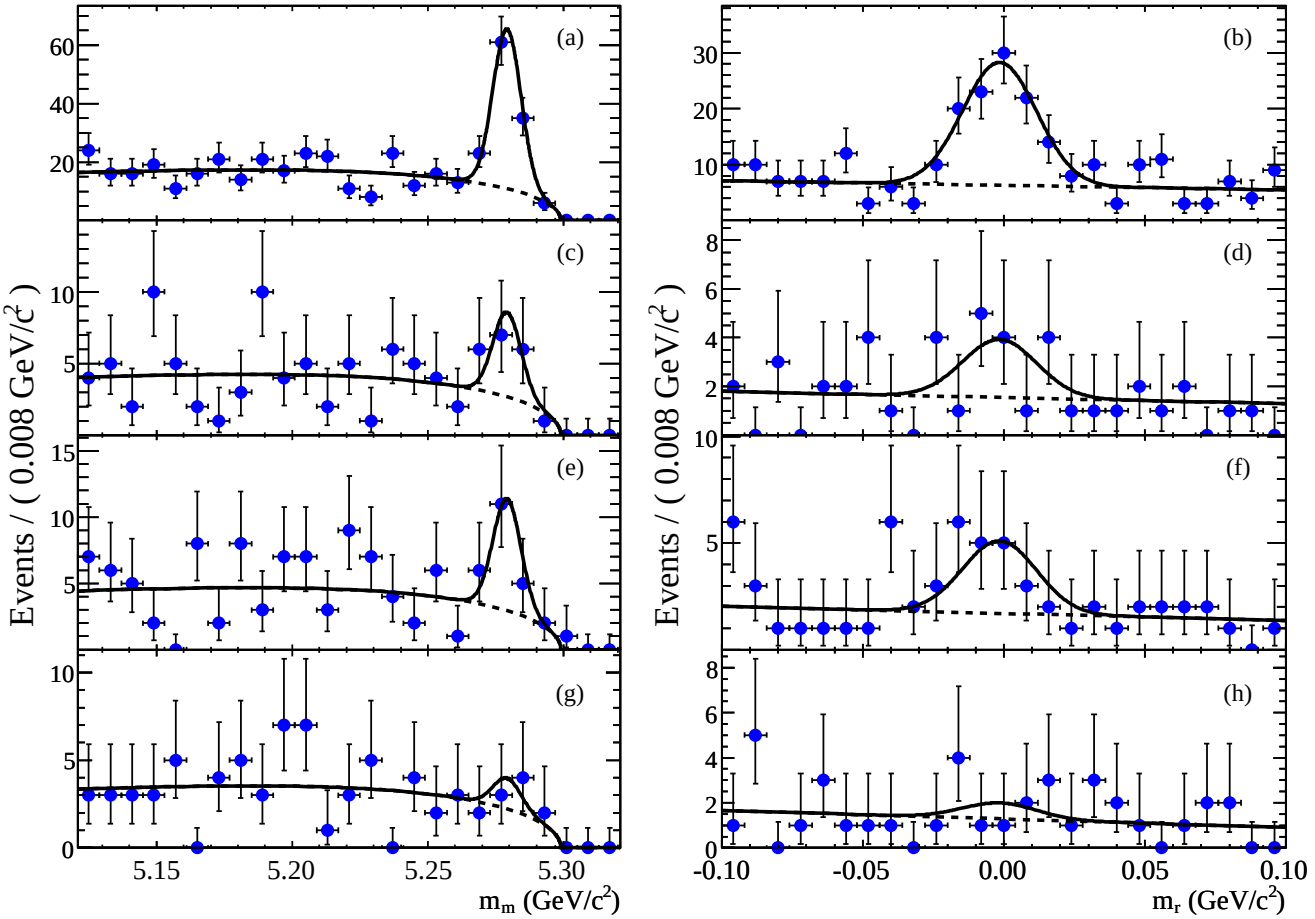

FIG. 1: Projections of m_m (left) and m_r (right) in data for $\overline{B}^0 \to \Lambda_c^+ \overline{p}$ candidates, separated by Λ_c^+ decay mode: (a, b) are $\Lambda_c^+ \to pK^-\pi^+$, (c, d) are $\Lambda_c^+ \to pK_S^0$, (e, f) are $\Lambda_c^+ \to pK_S^0\pi^+\pi^-$, and (g, h) are $\Lambda_c^+ \to \Lambda\pi^+$. The m_m projections (a, c, e, g) are for $|m_r| < 0.030\,\mathrm{GeV}/c^2$ and the m_r projections (b, d, f, h) are for $m_m > 5.27\,\mathrm{GeV}/c^2$. The solid curves correspond to the PDF from the simultaneous 2-D fit to candidates for the four Λ_c^+ decay modes, and the dashed curves represent the background component of the PDF.

measurements (x_l), is unbiased, and has the minimum possible variance $\hat{\sigma}^2$. The estimate $\hat{x}$ is defined by

$$\hat{x} = \sum_l \alpha_l x_l. \tag{8}$$

The condition $\sum_l \alpha_l = 1$ ensures that the method is unbiased. Each coefficient α_l is a constant weight for measurement x_l and is not necessarily positive. The set of coefficients $\boldsymbol{\alpha}$ (a vector with t elements) is determined by

$$\boldsymbol{\alpha} = \frac{\mathbf{E}^{-1}\,\mathbf{U}}{\mathbf{U}_T\,\mathbf{E}^{-1}\,\mathbf{U}}, \tag{9}$$

where $\mathbf{U}$ is a t-component vector whose elements are all 1 ($\mathbf{U}_T$ is its transpose) and $\mathbf{E}$ is the $(t \times t)$ error matrix. The diagonal elements of $\mathbf{E}$ are the individual variances, σ_l^2. The off-diagonal elements are the covariances between measurements ($r\sigma_l\sigma_{l'}$, where r is the correlation between measurements l and l'). The error matrices add linearly, so we define $\mathbf{E} = \mathbf{E}_{stat} + \mathbf{E}_{syst}$. $\mathbf{E}_{stat}$ includes the uncertainties in the fit yields and the correlations between yields from the simultaneous fit result. $\mathbf{E}_{syst}$ includes the systematic uncertainties that are described in the next section. Overall multiplicative constants ($N_{B\overline{B}}$ and $\mathcal{B}(\Lambda_c^+ \to pK^-\pi^+)$) that are common to all the measurements and their uncertainties are not included in the BLUE method.

The solutions for $\boldsymbol{\alpha}$ are

$\overline{B}^0 \to \Lambda_c^+ \overline{p}$:

$$\boldsymbol{\alpha}_T = \begin{pmatrix} 0.757 & 0.128 & 0.019 & 0.096 \end{pmatrix}, \tag{10}$$

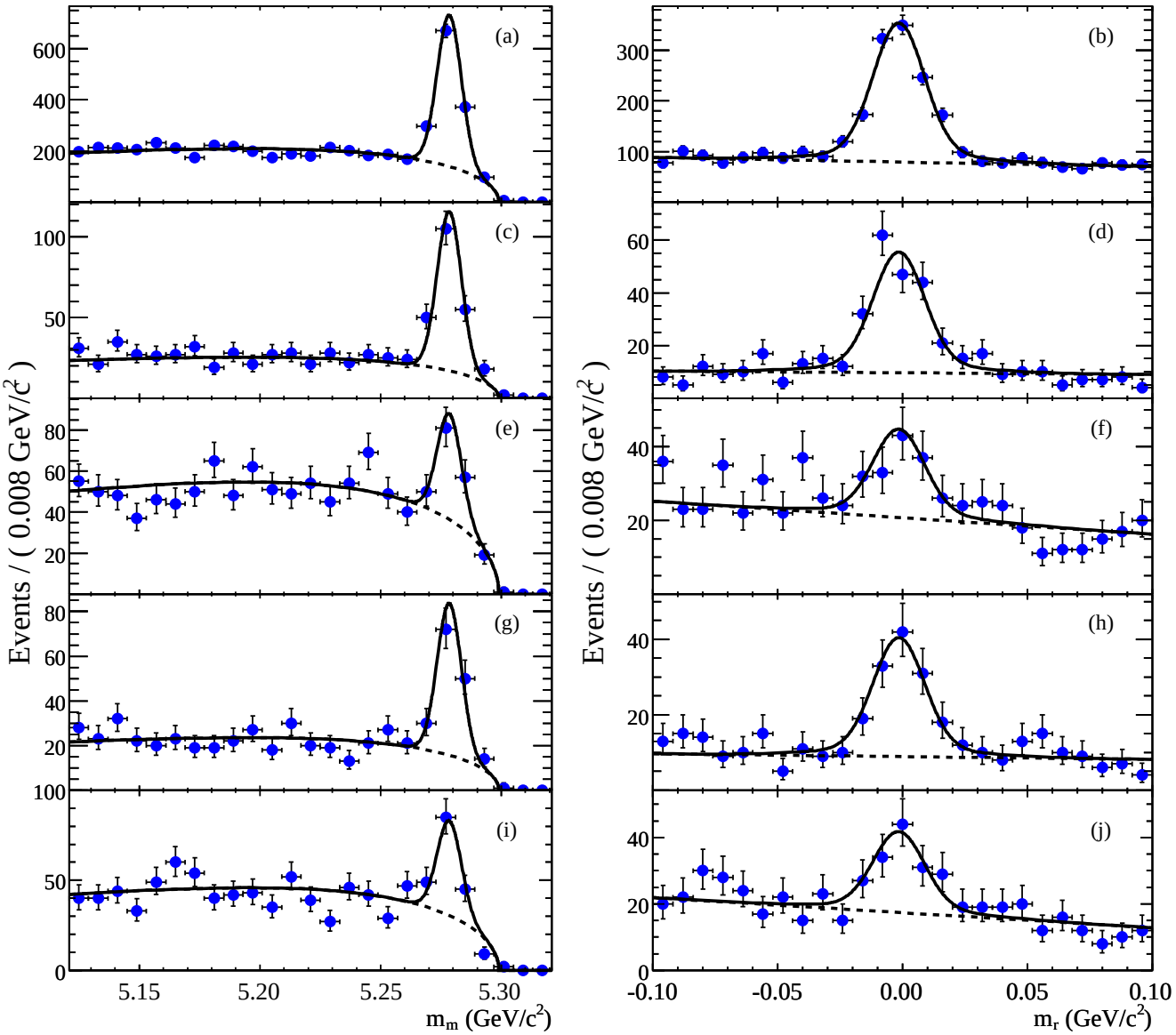

FIG. 2: Projections of m_m (left) and m_r (right) in data for $B^- \to \Lambda_c^+ \overline{p}\pi^-$ candidates, separated by Λ_c^+ decay mode: (a,b) are $\Lambda_c^+ \to pK^-\pi^+$, (c,d) are $\Lambda_c^+ \to pK_S^0$, (e,f) are $\Lambda_c^+ \to pK_S^0\pi^+\pi^-$, (g,h) are $\Lambda_c^+ \to \Lambda\pi^+$, and (i,j) are $\Lambda_c^+ \to \Lambda\pi^+\pi^-\pi^+$. The m_m projections (a,c,e,g,i) are for $|m_r| < 0.030\,\mathrm{GeV}/c^2$ and the m_r projections (b,d,f,h,j) are for $m_m > 5.27\,\mathrm{GeV}/c^2$. The solid curves correspond to the PDF from the simultaneous 2-D fit to candidates for the five Λ_c^+ decay modes, and the dashed curves represent the background component of the PDF.

and

$$B^- \to \Lambda_c^+ \overline{p}\pi^- :$$
$$\boldsymbol{\alpha}_T = \Big(\; 0.913 \;\; 0.043 \;\; -0.003 \;\; 0.029 \;\; 0.018 \; \Big), \quad (11)$$

where $\boldsymbol{\alpha}_T$ is the transpose of $\boldsymbol{\alpha}$. The order of the coefficients corresponds to the order of Λ_c^+ decay modes presented in Table III.

We calculate the best estimate $\hat{x}$ according to Eqn. 8 and divide this quantity by $N_{B\overline{B}}$ and $\mathcal{B}(\Lambda_c^+ \to pK^-\pi^+)$. We calculate the variance of $\hat{x}$

$$\hat{\sigma}^2 = \boldsymbol{\alpha}_T \, \mathbf{E} \, \boldsymbol{\alpha}. \quad (12)$$

Since the error matrices add linearly, we quote separate statistical and systematic uncertainties. The statistical and systematic uncertainties in $N_{B\overline{B}}$ are added in quadrature with the statistical and systematic $\hat{\sigma}$ results, respectively. The combined branching fraction measure-

ments are thus

$$\mathcal{B}(\overline{B}^0 \to \Lambda_c^+ \overline{p}) = (1.89 \pm 0.21 \pm 0.06 \pm 0.49) \times 10^{-5},$$
$$\mathcal{B}(B^- \to \Lambda_c^+ \overline{p}\pi^-) = (3.38 \pm 0.12 \pm 0.12 \pm 0.88) \times 10^{-4}, \quad (13)$$

where the uncertainties are statistical, systematic, and the uncertainty in $\mathcal{B}(\Lambda_c^+ \to pK^-\pi^+)$, respectively.

We use the same procedure to determine the branching ratio $\mathcal{B}(B^- \to \Lambda_c^+ \overline{p}\pi^-)/\mathcal{B}(\overline{B}^0 \to \Lambda_c^+ \overline{p})$:

$$\frac{\mathcal{B}(B^- \to \Lambda_c^+ \overline{p}\pi^-)}{\mathcal{B}(\overline{B}^0 \to \Lambda_c^+ \overline{p})} = 15.4 \pm 1.8 \pm 0.3. \quad (14)$$

In the branching ratio, many of the systematic uncertainties, including the dominant $\mathcal{B}(\Lambda_c^+ \to pK^-\pi^+)$ uncertainty, cancel.

SYSTEMATIC UNCERTAINTIES IN THE BRANCHING FRACTIONS

The uncertainties in the $\mathcal{B}(\overline{B}^0 \to \Lambda_c^+ \overline{p})$ and $\mathcal{B}(B^- \to \Lambda_c^+ \overline{p}\pi^-)$ measurements are dominated by the uncertainty in the $\Lambda_c^+ \to pK^-\pi^+$ branching fraction, and then by the uncertainties in the Λ_c^+ branching ratios (compared to $\Lambda_c^+ \to pK^-\pi^+$) [8].

The systematic uncertainties for each Λ_c^+ decay mode are summarized in Tables IV and V. The systematic uncertainty in the number of $B\overline{B}$ events is 1.1%.

The uncertainty in the efficiency determination is due to MC statistics, charged particle tracking, and particle identification. For $\overline{B}^0 \to \Lambda_c^+ \overline{p}$, the uncertainty due to MC statistics is $(0.4-0.6)\%$. For $B^- \to \Lambda_c^+ \overline{p}\pi^-$, we calculate the uncertainty due to MC statistics by independently varying the number of reconstructed signal MC events in each $\cos\theta_h, m_{\Lambda_c\pi}$ bin according to a Poisson distribution (ensuring that the data events in the same bin are correlated). The resulting uncertainty is $(0.6-3.1)\%$.

The tracking efficiency systematic uncertainties are determined from two separate studies. In the first study, $\tau^+\tau^-$ candidates are selected, in which one τ candidate decays to leptons and the other decays to more than one hadron plus a neutrino. Events are selected if one lepton and at least two charged hadrons are reconstructed. The efficiency is then measured for reconstructing the third charged particle for the hadronic decay. From this study there is a $(0.38-0.45)\%$ uncertainty in the tracking efficiency per charged particle. In the second method, a charged particle trajectory is reconstructed in the SVT, and then the efficiency for finding the corresponding trajectory in the DCH is measured. For the latter study, the uncertainties range from 0.21% to 1.18% depending on the Λ_c^+ decay mode. The systematic uncertainties determined in the two studies are added in quadrature.

The systematic uncertainty for charged particle identification is a measure of how well the corrections applied to the events in the signal MC sample for the efficiency determination describe the $\overline{B}^0 \to \Lambda_c^+ \overline{p}$ and $B^- \to \Lambda_c^+ \overline{p}\pi^-$ decay modes. The corrections are determined from control MC and data samples (a $\Lambda \to p\pi^-$ sample for protons and $D^{*+} \to D^0\pi^+, D^0 \to K^-\pi^+$ samples for pions and kaons). The efficiency as a function of momentum and angle for the $\overline{B}^0 \to \Lambda_c^+ \overline{p}$ and $B^- \to \Lambda_c^+ \overline{p}\pi^-$ signal MC samples and the control MC samples agree to within $(0.8-3.5)\%$ for different ranges of momentum and angle.

Systematic uncertainties due to the fit procedure are also considered. The dominant fit uncertainty is due to the threshold function parameter in the background PDF. The fit validation study showed that this parameter must be shared among Λ_c^+ decay modes to ensure fit robustness. We allowed this parameter to vary independently among Λ_c^+ decay modes and repeated the fit to data; the difference between the fit results is taken as a systematic uncertainty of $(1-24)\%$ depending on the Λ_c^+ decay mode. A peaking background due to misreconstructed $\overline{B}^0 \to \Sigma_c^+ \overline{p}, \Sigma_c^+ \to \Lambda_c^+ \pi^0$ events is present at the level of 1.0%. We assign a systematic uncertainty of 0.5% to account for the uncertainty in $\mathcal{B}(\overline{B}^0 \to \Sigma_c^+ \overline{p})$. The nominal endpoint in the fit to m_m is $5289.0\,\mathrm{MeV}/c^2$; we vary this by $\pm 0.5\,\mathrm{MeV}/c^2$, resulting in a systematic uncertainty of $(0.2-1.5)\%$.

$\Lambda_c^+ \overline{p}$ THRESHOLD ENHANCEMENT

The kinematic features and resonances in $B^- \to \Lambda_c^+ \overline{p}\pi^-$ are investigated through examination of the 2-D Dalitz plot ($m^2_{\overline{p}\pi}$ vs. $m^2_{\Lambda_c\pi}$) and its projections (the resonances will be discussed in the next section). Using the ${}_s\mathcal{P}lot$ formalism, we project the events in the $\{m_m, m_r\}$ fit region using the signal ${}_s\mathcal{P}lot$ weights and background ${}_s\mathcal{P}lot$ weights along with the efficiency corrections. This method allows us to project only the features of the signal events, while taking the efficiency variations into account. Figure 3 shows the ${}_s\mathcal{P}lot$ weights for $m^2_{\overline{p}\pi}$ vs. $m^2_{\Lambda_c\pi}$. Note that the negative bins are suppressed in the 2-D Dalitz plot.

We project the events in the fit region onto the $m_{\Lambda_c\overline{p}}$ axis with signal ${}_s\mathcal{P}lot$ weights and efficiency corrections to study the enhancement at threshold in the baryon-antibaryon mass distribution. This enhancement can be seen in $B^- \to \Lambda_c^+ \overline{p}\pi^-$ decays as a peak in $m_{\Lambda_c\overline{p}}$ near the kinematic threshold, $m^0_{\Lambda_c\overline{p}} = 3224.8\,\mathrm{MeV}/c^2$. We divide the normalized $m_{\Lambda_c\overline{p}}$ distribution by the expectation from three-body phase-space; the resulting distribution is shown in Figure 4. An enhancement is clearly visible near threshold. The observation of this enhancement is consistent with baryon-antibaryon threshold enhancements as seen in other decay modes such as $B \to p\overline{p}K$,

TABLE III: Summary of the individual and combined branching fraction measurements for $\overline{B}^0 \to \Lambda_c^+ \overline{p}$ and $B^- \to \Lambda_c^+ \overline{p}\pi^-$. The uncertainties are statistical, systematic, and due to $\mathcal{B}(\Lambda_c^+ \to pK^-\pi^+)$, respectively.

Mode	$\mathcal{B}(\overline{B}^0 \to \Lambda_c^+ \overline{p})$	$\mathcal{B}(B^- \to \Lambda_c^+ \overline{p}\pi^-)$
$\Lambda_c^+ \to pK^-\pi^+$	$(2.05 \pm 0.25 \pm 0.05 \pm 0.53) \times 10^{-5}$	$(3.38 \pm 0.13 \pm 0.11 \pm 0.88) \times 10^{-4}$
$\Lambda_c^+ \to pK_S^0$	$(1.49 \pm 0.60 \pm 0.17 \pm 0.39) \times 10^{-5}$	$(3.82 \pm 0.35 \pm 0.38 \pm 0.99) \times 10^{-4}$
$\Lambda_c^+ \to pK_S^0\pi^+\pi^-$	$(4.33 \pm 1.55 \pm 0.57 \pm 1.13) \times 10^{-5}$	$(4.58 \pm 0.70 \pm 0.66 \pm 1.19) \times 10^{-4}$
$\Lambda_c^+ \to \Lambda\pi^+$	$(0.71 \pm 0.71 \pm 0.18 \pm 0.18) \times 10^{-5}$	$(3.98 \pm 0.45 \pm 0.39 \pm 1.03) \times 10^{-4}$
$\Lambda_c^+ \to \Lambda\pi^+\pi^-\pi^+$	–	$(3.49 \pm 0.51 \pm 0.38 \pm 0.91) \times 10^{-4}$
combined	$(1.89 \pm 0.21 \pm 0.06 \pm 0.49) \times 10^{-5}$	$(3.38 \pm 0.12 \pm 0.12 \pm 0.88) \times 10^{-4}$

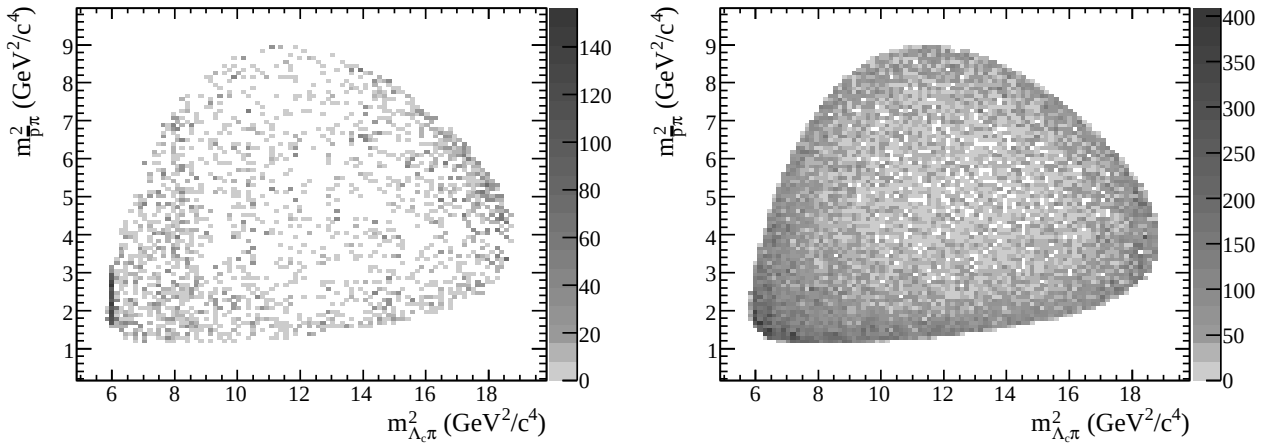

FIG. 3: Dalitz plot of $m^2_{\overline{p}\pi}$ vs. $m^2_{\Lambda_c\pi}$. Each event is efficiency-corrected and given a signal (left) or background (right) ${}_s\mathcal{P}lot$ weight. Note that the density scales on the left- and right-hand plots are different, and negative bins are suppressed.

$B \to Dp\overline{p}(\pi)$, or in continuum $e^+e^- \to p\overline{p}\gamma$ [1, 2].

RESONANT SUBSTRUCTURE OF $B^- \to \Lambda_c^+ \overline{p}\pi^-$

We also project the events in the fit region onto the $m_{\Lambda_c\pi}$ axis with signal ${}_s\mathcal{P}lot$ weights and efficiency corrections to study resonances in $m_{\Lambda_c\pi}$. We perform 1-D binned χ^2 fits to discriminate between resonant ($B^- \to \Sigma_c^0\ \overline{p}$) and nonresonant ($B^- \to \Lambda_c^+ \overline{p}\pi^-$) signal events. In each binned χ^2 fit, the PDF is numerically integrated over each (variable-sized) bin and the following quantity is minimized:

$$\chi^2 = \sum_{i=1}^{n_{\rm bins}} \left(\frac{\int \left(Y_{\rm sig}\mathcal{P}_{\rm sig} + Y_{\rm nr}\mathcal{P}_{\rm nr}\right)\, dm_i \ - \ Y_i}{\sigma_i} \right)^2, \quad (15)$$

where $\mathcal{P}_{\rm sig}$ is the resonant signal PDF, $\mathcal{P}_{\rm nr}$ is the nonresonant signal PDF, $Y_{\rm sig}$ is the expected yield of weighted resonant signal events, and $Y_{\rm nr}$ is the expected yield of weighted nonresonant signal events. We assume the amplitude and phase of the non-resonant $B^- \to \Lambda_c^+ \overline{p}\pi^-$ contribution is constant over the Dalitz plot, and does not interfere with the resonant contributions. The range of the integral over the quantity dm_i takes into account the variable bin width, Y_i is the number of weighted data events, and σ_i is the uncertainty in Y_i. Variable bin widths are used to ensure that there are a sufficient number of signal events in each $m_{\Lambda_c\pi}$ bin so that the estimated uncertainty is valid. This is especially important in the non-resonant sideband regions. Bin widths in the signal regions are chosen to have sufficient granularity throughout the resonant peaks.

The $\Sigma_c(2455)^0$ and $\Sigma_c(2520)^0$ are well-established resonances that decay to $\Lambda_c^+\pi^-$. A third Σ_c resonance, the $\Sigma_c(2800)^0$, was reported by the Belle Collaboration in 2005 [29] along with its isospin partners $\Sigma_c(2800)^+$ and $\Sigma_c(2800)^{++}$. These resonances were observed in continuum ($e^+e^- \to c\overline{c}$) $\Lambda_c\pi$ events. The $\Sigma_c(2800)^0$ resonance was fit with a D-wave Breit-Wigner distribution and the mass difference $\Delta m = m_{\Sigma_c(2800)^0} - m_{\Lambda_c^+} = (515 \pm 3\,{}^{+\,2}_{-\,6})\,\mathrm{MeV}/c^2$ was measured, which corresponds to an absolute mass of $(2802\,{}^{+\,4}_{-\,7})\,\mathrm{MeV}/c^2$ [8]. The natural width of the resonance is $(61^{+\,28}_{-\,18})\,\mathrm{MeV}$ [29]. We search for evidence of all three resonances.

TABLE IV: Summary of the contributions to the relative systematic uncertainty in $\mathcal{B}(\overline{B}^0 \to \Lambda_c^+ \overline{p})$ for each Λ_c^+ decay mode. The total for each mode is determined by adding the uncertainty from each source in quadrature. The fractional statistical uncertainty in the fit yield for each mode is provided for comparison.

Source	$\overline{B}^0 \to \Lambda_c^+ \overline{p}$ Systematic Uncertainty			
	$\Lambda_c^+ \to pK^-\pi^+$	$\Lambda_c^+ \to pK_S^0$	$\Lambda_c^+ \to pK_S^0\pi^+\pi^-$	$\Lambda_c^+ \to \Lambda\pi^+$
$B\overline{B}$ events	1.1%	1.1%	1.1%	1.1%
$\mathcal{R}_l$	–	8.5%	11.8%	8.9%
MC statistics	0.4%	0.6%	0.6%	0.4%
Tracking	1.7%	1.9%	2.8%	1.7%
Displaced Vertices	–	1.1%	1.1%	1.1%
Particle Identification	1.5%	2.1%	1.7%	1.6%
Fitting	0.9%	7.0%	4.9%	24.2%
Total	3%	12%	13%	26%
Statistical	12%	40%	36%	100%

TABLE V: Summary of the contributions to the relative systematic uncertainty in $\mathcal{B}(B^- \to \Lambda_c^+ \overline{p}\pi^-)$ for each Λ_c^+ decay mode. The total for each mode is determined by adding the uncertainty from each source in quadrature. The fractional statistical uncertainty in the fit yield for each mode is provided for comparison.

Source	$B^- \to \Lambda_c^+ \overline{p}\pi^-$ Systematic Uncertainty				
	$\Lambda_c^+ \to pK^-\pi^+$	$\Lambda_c^+ \to pK_S^0$	$\Lambda_c^+ \to pK_S^0\pi^+\pi^-$	$\Lambda_c^+ \to \Lambda\pi^+$	$\Lambda_c^+ \to \Lambda\pi^+\pi^-\pi^+$
$B\overline{B}$ events	1.1%	1.1%	1.1%	1.1%	1.1%
$\mathcal{R}_l$	–	8.5%	11.8%	8.9%	6.1%
MC statistics	0.6%	2.1%	3.1%	2.0%	3.0%
Tracking	2.6%	2.3%	3.2%	2.1%	2.9%
Displaced Vertices	–	1.1%	1.1%	1.1%	1.1%
Particle Identification	0.8%	1.8%	2.5%	1.8%	3.5%
Fitting	1.6%	3.2%	6.5%	2.5%	2.4%
Total	3.4%	9.9%	14.5%	10.0%	8.7%
Statistical	4.5%	9.1%	16.3%	11.4%	14.8%

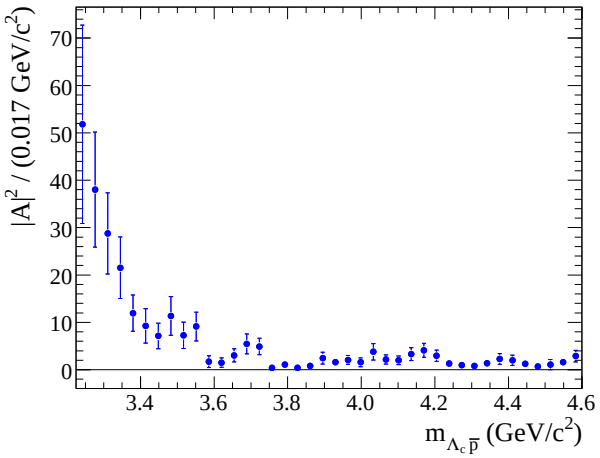

FIG. 4: Projection of the amplitude squared ($|A|^2$) vs. $m_{\Lambda_c \overline{p}}$ for $B^- \to \Lambda_c^+ \overline{p} \pi^-$ decays near threshold. Candidates are efficiency-corrected, weighted using the ${}_s\mathcal{P}lot$ technique, and corrected according to three-body phase space.

A significant $\Sigma_c(2455)^0$ signal is seen near threshold; see Fig. 3 and Fig. 5. We construct a resonant signal PDF from a non-relativistic S-wave Breit-Wigner distribution convolved with the sum of two Gaussian distributions (to form a "Voigtian" distribution). This quantity is multiplied by a phase-space function. The mass and (constant) width of the resonance in the Breit-Wigner PDF are free in the fit. The resolution (described by the two Gaussians) is fixed; it is determined from a $B^- \to \Sigma_c(2455)^0 \overline{p}$, $\Sigma_c(2455)^0 \to \Lambda_c^+ \pi^-$, $\Lambda_c^+ \to pK^-\pi^+$ signal MC sample by comparing the measured $\Sigma_c(2455)^0$ mass to the true $\Sigma_c(2455)^0$ mass for each candidate. The two-body phase-space function goes to zero at the kinematic threshold for $\Lambda_c \pi$: 2426.03 MeV/c^2. The non-resonant signal PDF is a threshold function [26]; the threshold is set to the kinematic threshold for $\Lambda_c \pi$. The shape parameter for the threshold function is fixed from a fit to a non-resonant $B^- \to \Lambda_c^+ \overline{p} \pi^-$ signal MC sample. The weighted data points are shown in Fig. 5 with the fit overlaid; the fit results are summarized in Table VI. The average efficiency for $\Lambda_c^+ \to pK^-\pi^+$ signal MC events in this region is 14.1%.

No significant signal is seen in the region of the $\Sigma_c(2520)^0$; see Fig. 6. We perform a fit using a relativistic D-wave Breit-Wigner distribution with a mass-dependent width to describe the resonant signal PDF, fixing the resonance mass and the width to the world average values [8]: $m_R = (2518.0 \pm 0.5)$ MeV/c^2 and $\Gamma_R = (16.1 \pm 2.1)$ MeV. The non-resonant signal PDF is a first-order polynomial. We obtain $Y_{\rm sig} = 27 \pm 69$ events; the fit result is shown in Fig. 6. The average efficiency for $\Lambda_c^+ \to pK^-\pi^+$ signal MC events in this region is 15.4%.

In the $m_{\Lambda_c \pi}$ distribution, we also observe an excited

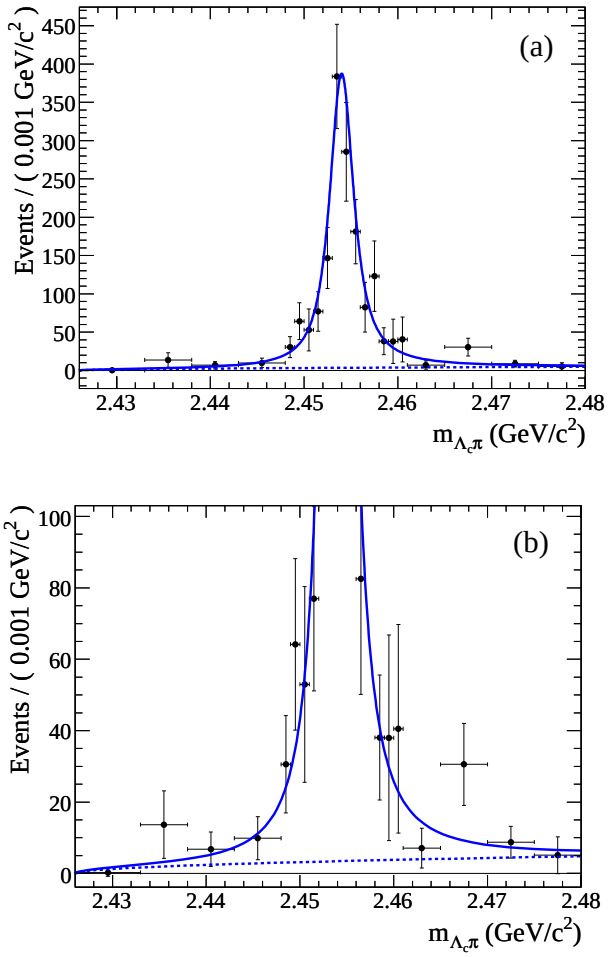

FIG. 5: (a) Projection of $m_{\Lambda_c \pi}$ showing the $\Sigma_c(2455)^0$ resonance. Events are efficiency corrected and weighted using the ${}_s\mathcal{P}lot$ technique, and the result of a binned χ^2 fit to a Voigtian signal plus a threshold function background is overlaid. The variable bin sizes range from 1 to 7 MeV/c^2. (b) The same fit result and data is shown on a smaller vertical scale to show the behavior of the PDF at threshold.

TABLE VI: Fit results for $B^- \to \Sigma_c(2455)^0 \overline{p}$. $Y_{\rm sig}$ is the efficiency-corrected resonant signal yield in the fit range. Systematic uncertainties from the fit to m_m vs. m_r are not included in the yield. The world average values from the Particle Data Group (PDG) of the mass and width of the $\Sigma_c(2455)^0$ are included for comparison [8].

Fit Parameter	Value	PDG Value [8]
$Y_{\rm sig}$	1522 ± 149	
m_R (GeV/c^2)	2.4540 ± 0.0002	2.4538 ± 0.0002
Γ_R (MeV)	2.6 ± 0.5	2.2 ± 0.4

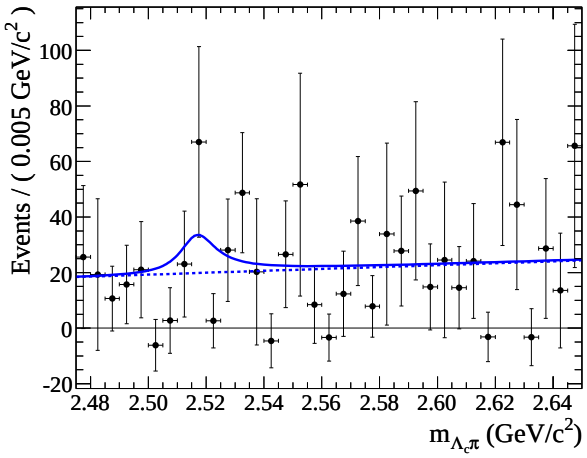

FIG. 6: Projection of $m_{\Lambda_c\pi}$ in the region of the $\Sigma_c(2520)^0$ resonance. Events are efficiency corrected and weighted using the ${}_s\mathcal{P}lot$ technique, and the result of a binned χ^2 fit to a relativistic D-wave Breit-Wigner signal with a mass-dependent width plus a linear background is overlaid. The bin size is $5\,\mathrm{MeV}/c^2$. No significant signal is seen.

Σ_c^0 state that is higher in mass than the $\Sigma_c(2520)^0$. We construct a resonant signal PDF from a relativistic Breit-Wigner distribution with a mass-dependent width:

$$\Gamma(q) = \Gamma_R \left(\frac{q}{q_R}\right)^{2L+1} \left(\frac{m_R}{m_{\Lambda_c\pi}}\right) B'_L(q, q_R)^2. \qquad (16)$$

The quantity L is the angular momentum ($L = 0, 1, 2$ is S-wave, P-wave, D-wave, respectively), q is the momentum of the Λ_c^+ (which is equal to the momentum of the π^-) in the excited Σ_c^0 rest frame, and q_R is the value of q when $m_{\Lambda_c\pi} = m_R$. In Eqn. 16, $B'_L(q, q_R)$ is the Blatt-Weisskopf barrier factor [8]:

$$\begin{aligned} B'_0(q, q_R) &= 1, \\ B'_1(q, q_R) &= \sqrt{\frac{1 + q_R^2\, d^2}{1 + q^2\, d^2}}, \\ B'_2(q, q_R) &= \sqrt{\frac{(q_R^2\, d^2 - 3)^2 + 9 q_R^2\, d^2}{(q^2\, d^2 - 3)^2 + 9 q^2\, d^2}}, \end{aligned} \qquad (17)$$

where we define a constant impact parameter $d = 1\,\mathrm{fm}$ (the approximate radius of a baryon), which corresponds to $5.1\,\mathrm{GeV}^{-1}$. Blatt-Weisskopf barrier factors are weights that account for the fact that the maximum angular momentum (L) in a strong decay is limited by the linear momentum (q). Since the resonance is quite wide, we do not need to include a resolution function in the resonant signal PDF. The two fit parameters (m_R and Γ_R) of the Σ_c^0 are free in the fit. The non-resonant signal PDF is a first-order polynomial.

From the 1-D binned χ^2 fit, we obtain $Y_{\mathrm{sig}} = 1449 \pm 284$ efficiency-corrected events for the excited Σ_c^0 state. We choose $L = 2$ for the nominal fit, but investigate $L = 0, 1$ as well. The average efficiency for $\Lambda_c^+ \to pK^-\pi^+$ signal MC events in this region is 16.3%. The fit results are summarized in Table VII and shown in Fig. 7. The χ^2 from the fit is 37 with 31 degrees of freedom (DOF). If the signal yield is fixed to zero and the mean and width are fixed to the central values from the nominal fit, the resulting χ^2 is 78 with 34 DOF. The significance can be calculated from $\Delta\chi^2 = 40.9$, which is equivalent to 5.8σ for the joint estimation of three parameters.

The measured width of this state $(86\,^{+\,33}_{-\,22} \pm 12)\,\mathrm{MeV}$ is consistent with the width of the $\Sigma_c(2800)^0$ measured by Belle [29]. However, the measured mass of this excited Σ_c^0 is $(2846 \pm 8 \pm 10)\,\mathrm{MeV}/c^2$, which is $40\,\mathrm{MeV}/c^2$ and 3σ higher (assuming Gaussian statistics) than Belle's measured mass for the $\Sigma_c(2800)^0$.

We evaluate systematic uncertainties for the $\Sigma_c(2455)^0$ and the excited Σ_c^0 yields, masses, and widths by modifying the binning, the resonant signal PDF shape, and the

TABLE VII: Fit results for the excited Σ_c^0 resonance. Y_{sig} is the efficiency-corrected resonant signal yield in the fit range. Systematic uncertainties from the fit to m_m vs. m_r are not included in the yield. The world average values from the Particle Data Group (PDG) of the mass and width of the $\Sigma_c(2800)^0$ are included for comparison [8].

Fit Parameter	Value	PDG Value [8]
Y_{sig}	1449 ± 284	
m_R (GeV/c^2)	2.846 ± 0.008	$2.802\,^{+\,0.004}_{-\,0.007}$
Γ_R (MeV)	$86\,^{+\,33}_{-\,22}$	$61\,^{+\,28}_{-\,18}$

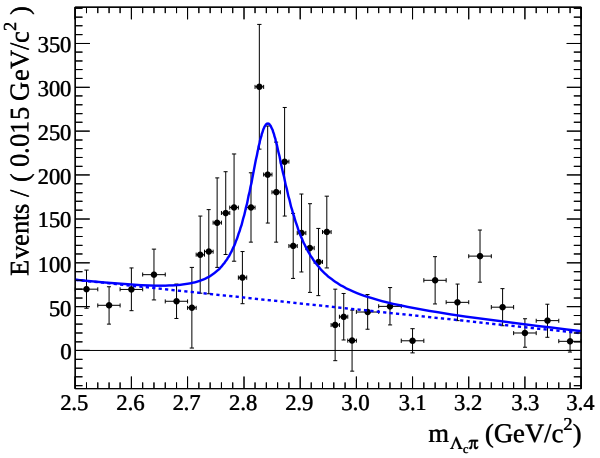

FIG. 7: Projection of $m_{\Lambda_c\pi}$ showing an excited Σ_c^0 resonance. Events are efficiency corrected and weighted using the ${}_s\mathcal{P}lot$ technique. The result of a binned χ^2 fit to a relativistic D-wave Breit-Wigner signal with a mass-dependent width plus a linear background is overlaid. The variable bin sizes range from 15 to $40\,\mathrm{MeV}/c^2$.

TABLE VIII: Systematic uncertainties for $Y_{\rm sig}$, m_R (in MeV/c^2), and Γ_R (in MeV) for the $\Sigma_c(2455)^0$ and excited Σ_c^0 resonances.

	$\Sigma_c(2455)^0$		excited Σ_c^0		
Systematic Source	$Y_{\rm sig}$	Γ_R	$Y_{\rm sig}$	m_R	Γ_R
Resonant Signal PDF	–	–	5.9%	–	$\pm$ 7
Non-resonant Signal PDF	–	–	1.2%	–	$\pm$ 2
Binning	6.9%	$\pm$0.3	20%	$\pm$10	$\pm$10
Total	6.9%	$\pm$0.3	21%	$\pm$10	$\pm$12

non-resonant signal PDF shape. Changing the variable bin sizes leads to the dominant systematic uncertainty in the masses, widths, and yields of both resonances. For the $\Sigma_c(2455)^0$, the bin width in the peak region was decreased from the nominal $1\,{\rm MeV}/c^2$ to $0.5\,{\rm MeV}/c^2$; for the excited Σ_c^0, the bin width was varied from 10 to $20\,{\rm MeV}/c^2$ compared to the nominal $15\,{\rm MeV}/c^2$. For both resonances, an S-wave and a P-wave relativistic Breit-Wigner (without a resolution function) was used instead of the nominal resonant signal PDF. The (fixed) non-resonant threshold parameter for the $\Sigma_c(2455)^0$ was varied by $\pm1\sigma$. A second-order polynomial was used (instead of a first-order polynomial) for the excited Σ_c^0 non-resonant PDF. A summary of the systematic uncertainties for $Y_{\rm sig}$, m_R, and Γ_R are summarized in Table VIII.

The significance is recalculated following each of the variations used to evaluate the systematic uncertainties in the excited Σ_c^0 resonance parameters. The resulting significance (including systematics) is 5.2σ. A cross-check is performed to make sure the $\Sigma_c(2800)^0$ signal is not the result of interference with a $\Delta(1232)^{++}$, for example (although no significant $\Delta(1232)^{++}$ signal is seen in the $m_{\overline{p}\pi}$ distribution). The fit is performed again in the $\Sigma_c(2800)^0$ mass region for candidates with $m_{\overline{p}\pi} > 1.5\,{\rm GeV}/c^2$. We obtain 1329 ± 230 resonant signal events (compared to 1449 ± 284 events for the nominal fit) and a consistent mass and width.

An additional cross-check is performed to investigate whether there are appropriate fractions of resonant $\Sigma_c(2800)^0$ events in different Λ_c^+ decay modes. This is accomplished by dividing the ${}_s\mathcal{P}lot$-weighted, efficiency-corrected data into two samples according to the Λ_c^+ decay mode. Note that this cross-check neglects statistical correlations from the combined m_r vs. m_m fit (less than 15%) among the Λ_c^+ decay modes. A binned χ^2 fit to only $\Lambda_c^+ \to pK^-\pi^+$ candidates gives $Y_{\rm sig} = 776 \pm 160$, compared to 6463 ± 241 total non-resonant $B^- \to \Lambda_c^+\overline{p}\pi^-$, $\Lambda_c^+ \to pK^-\pi^+$ events ($(12 \pm 3)\%$). A binned χ^2 fit to a combined sample of $\Lambda_c^+ \to pK_S^0$, $\Lambda_c^+ \to pK_S^0\pi^+\pi^-$, $\Lambda_c^+ \to \Lambda\pi^+$, and $\Lambda_c^+ \to \Lambda\pi^+\pi^-\pi^+$ candidates gives $Y_{\rm sig} = 530 \pm 177$ compared to 5956 ± 431 non-resonant events ($(9 \pm 3)\%$). (In order for this fit to converge, m_R and Γ_R were fixed to their nominal values.) The fractions are consistent in the two samples and the total (1306 ± 239 events) is consistent with the nominal fit result within uncertainties.

We have also investigated the possibility that there are two resonances in the mass range shown in Figure 7. However, there is no evidence for two distinct vertical bands in this region in the $B^- \to \Lambda_c^+\overline{p}\pi^-$ Dalitz plot (Figure 3), and we do not obtain a statistically significant fit to two resonances.

In order to measure the fraction of $B^- \to \Lambda_c^+\overline{p}\pi^-$ decays that proceed through intermediate Σ_c resonances, we assume that the contribution from each Λ_c^+ decay mode for events in the Σ_c regions is equal to the measured contribution from each Λ_c^+ decay mode in all (resonant and non-resonant) $B^- \to \Lambda_c^+\overline{p}\pi^-$ events. We set a 90% C.L. upper limit on $B^- \to \Sigma_c(2520)^0\overline{p}$ that includes systematic uncertainties and corresponds to 109 events. The measured fractions or upper limits of $B^- \to \Lambda_c^+\overline{p}\pi^-$ decays that proceed through an intermediate Σ_c resonance are

$$\begin{aligned}
\frac{\mathcal{B}(B^- \to \Sigma_c(2455)^0\overline{p})}{\mathcal{B}(B^- \to \Lambda_c^+\overline{p}\pi^-)} &= (12.3 \pm 1.2 \pm 0.8) \times 10^{-2},\\
\frac{\mathcal{B}(B^- \to \Sigma_c(2800)^0\overline{p})}{\mathcal{B}(B^- \to \Lambda_c^+\overline{p}\pi^-)} &= (11.7 \pm 2.3 \pm 2.4) \times 10^{-2},\\
\frac{\mathcal{B}(B^- \to \Sigma_c(2520)^0\overline{p})}{\mathcal{B}(B^- \to \Lambda_c^+\overline{p}\pi^-)} &< 0.9 \times 10^{-2}\,(90\%\ {\rm C.L.}).
\end{aligned} \tag{18}$$

Therefore approximately 1/4 of $B^- \to \Lambda_c^+\overline{p}\pi^-$ decays proceed through a known intermediate Σ_c resonance.

MEASUREMENT OF THE $\Sigma_c(2455)^0$ SPIN

The $\Sigma_c(2455)^0$ is the lowest mass Σ_c state. In the quark model, it is expected to have $J^P = \frac{1}{2}^+$, where J is the spin and P is the parity. In this section, we provide a quantitative evaluation of the spin-1/2 and spin-3/2 hypotheses for the $\Sigma_c(2455)^0$ baryon.

We determine the spin of the $\Sigma_c(2455)^0$ through an angular analysis of the decay $B^- \to \Sigma_c(2455)^0\overline{p}$, $\Sigma_c(2455)^0 \to \Lambda_c^+\pi^-$. We define a helicity angle θ_h as the angle between the momentum vector of the Λ_c^+ and the momentum vector of the recoiling B-daughter $\overline{p}$ in the rest frame of the $\Sigma_c(2455)^0$. If we assume $J(\Lambda_c^+) = 1/2$, the angular distributions for the spin-1/2 and spin-3/2 hypotheses for the $\Sigma_c(2455)^0$ are

$$\begin{aligned}
J(\Sigma_c^0) = \frac{1}{2}: &\quad \frac{dN}{d\cos\theta_h} \propto 1\\
J(\Sigma_c^0) = \frac{3}{2}: &\quad \frac{dN}{d\cos\theta_h} \propto 1 + 3\cos^2\theta_h.
\end{aligned} \tag{19}$$

These are the ideal distributions; the measured angular distributions will be somewhat degraded due to nonuni-

form detector efficiencies, finite experimental resolution for measuring θ_h, and background contamination. We estimate the effects of inefficiencies and background contamination by performing parameterized MC studies to quantify the decrease in sensitivity to discriminate between possible spin values.

If we select from a $\pm 2\sigma$ signal region in m_m and m_r, without ${}_s\mathcal{P}lot$ weights or efficiency corrections, there are 127 events in the $\Sigma_c(2455)^0$ signal region and 27 events in the $\Sigma_c(2455)^0$ background regions ($2.430 < m_{\Lambda_c\pi} < 2.445\,\mathrm{GeV}/c^2$ and $2.463 < m_{\Lambda_c\pi} < 2.478\,\mathrm{GeV}/c^2$). Scaling the number of events in the background region by the ratio of the total width of the background regions compared to the width of the signal region, we expect 7.2 ± 1.3 background events in the signal region.

We measure the finite experimental resolution of $\cos\theta_h$ by comparing the measured value of $\cos\theta_h$ to the true value of $\cos\theta_h$ in $B^- \to \Lambda_c^+ \overline{p}\pi^-, \Lambda_c^+ \to pK^-\pi^+$ events in a signal MC sample. The maximum root mean square of the measured value of $\cos\theta_h$ minus the true value of $\cos\theta_h$ in the $\Sigma_c(2455)^0$ signal region determines the helicity angle resolution $\sigma(\cos\theta_h) < 0.03$. Therefore the finite experimental resolution is small compared to any features in the spin-1/2 or spin-3/2 angular distributions.

We investigate the discrimination power between spin hypotheses using parameterized MC studies. In general, the log likelihood is computed as $\ln\mathcal{L} = \sum_i w_i \ln(y_i)$, where y_i is the probability density for observing event i. The weight w_i for the MC studies is $w_i = \varepsilon_i$, where ε_i is the efficiency for event i. We compute a log likelihood for each hypothesis:

$$\begin{aligned} \ln\mathcal{L}(1/2) &= \sum_i w_i \ln\frac{1}{2} \\ \ln\mathcal{L}(3/2) &= \sum_i w_i \ln\left[\frac{1}{4}\left(1+3\cos^2\theta_{h,i}\right)\right]. \end{aligned} \tag{20}$$

The shape of the $\cos\theta_h$ distribution for background events is estimated from the shape of the helicity distribution for events in the background regions. The helicity distribution for these events is illustrated in Fig. 8 as a non-parametric PDF (a histogram). This PDF is used to generate the number of background events in the signal region with a Poisson uncertainty (7.2 ± 2.7). The total number of events in the sample is fixed to 127, so the background effectively dilutes the signal distribution.

We then generate 500 samples (127 events each) and compute the likelihood $\mathcal{L}$ that each generated distribution is uniform in $\cos\theta_h$ (spin-1/2) or distributed as $1+3\cos^2\theta_h$ (spin-3/2). We define the quantity $\Delta\ln\mathcal{L} = \ln\mathcal{L}(1/2) - \ln\mathcal{L}(3/2)$. Figure 9 shows the distribution $\Delta\ln\mathcal{L}$ for events generated with each hypothesis. The dashed histogram (negative values of $\Delta\ln\mathcal{L}$) corresponds to samples generated according to the spin-3/2 hypothesis, and the solid histogram (positive values of $\Delta\ln\mathcal{L}$) corresponds to samples generated according to the spin-1/2 hypothesis. For each distribution, the separation from zero illustrates how well we can discriminate between hypotheses given 127 signal events.

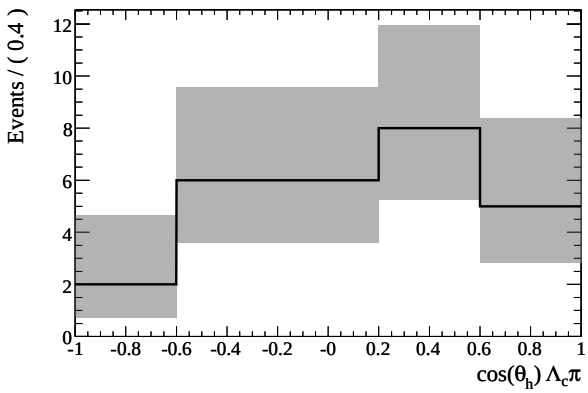

FIG. 8: Helicity angle distribution for the combined sample of background and non-resonant signal events, a non-parameteric PDF (line). The shaded region indicates the Poisson uncertainty in the distribution.

The helicity angle distribution for events in the signal region around the $\Sigma_c(2455)^0$ is shown in Figure 10. The points are efficiency-corrected. Functions corresponding to the spin-1/2 (solid) and spin-3/2 (dashed) hypotheses are overlaid. We compute the difference in log likelihood between the hypotheses: $\Delta\ln\mathcal{L} = +19.2$. We indicate the value of $\Delta\ln\mathcal{L}$ in data with a vertical line in Figure 9. The observed value of $\Delta\ln\mathcal{L}$ is consistent with the spin-1/2 hypothesis and excludes the spin-3/2 hypothesis at the $> 4\sigma$ level.

The ideal angular distributions for the $\Sigma_c(2455)^0$ stated in Eqn. 19 are also applicable for the excited Σ_c^0 resonance. Unlike the narrow $\Sigma_c(2455)^0$ resonance near threshold, the excited Σ_c^0 is much wider and therefore its angular distribution is extremely contaminated by the non-resonant signal events underneath the signal. We perform a non-resonant sideband subtraction to extract the helicity angle distribution of the excited Σ_c^0, but are limited by the number of signal events available. An examination of this distribution is somewhat consistent with a $J = 1/2$ hypothesis, but no conclusive statement can be made about the spin of the observed excited Σ_c^0.

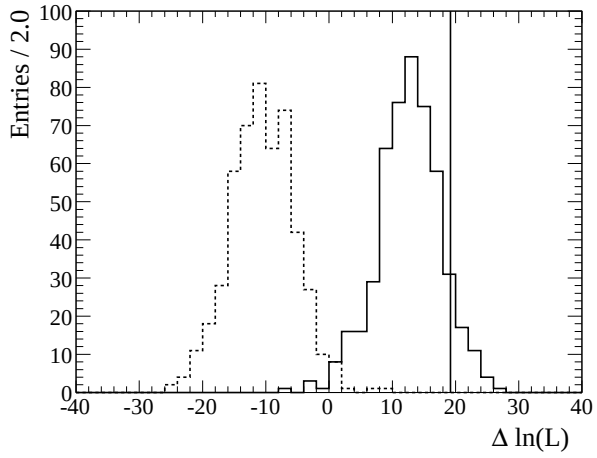

FIG. 9: Distribution of $\Delta \ln \mathcal{L} = \ln \mathcal{L}(1/2) - \ln \mathcal{L}(3/2)$ for signal events generated with a uniform distribution in $\cos\theta_h$ (solid histogram, positive values) and a $1 + 3\cos^2\theta_h$ distribution (dashed histogram, negative values). Background events are included, and all events are efficiency-corrected. We measure $\Delta \ln \mathcal{L} = +19.2$ in data (indicated by the vertical line), so we accept the spin-1/2 hypothesis.

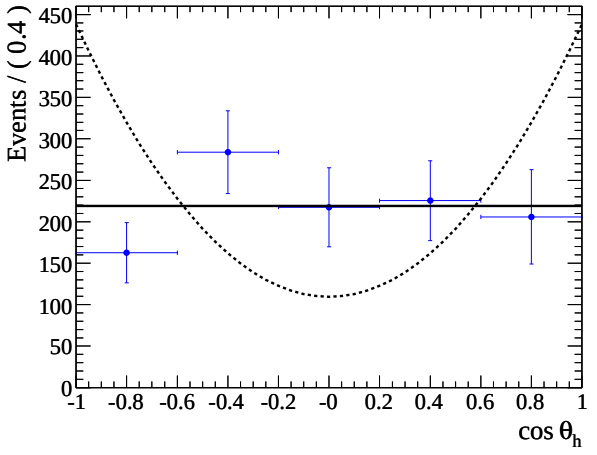

FIG. 10: The helicity angle distribution for $\Sigma_c(2455)^0$ candidates in data. The points correspond to efficiency-corrected $B^- \to \Sigma_c(2455)^0\overline{p}$ candidates. The curves for the spin-1/2 (solid line) and spin-3/2 (dashed line) hypotheses are overlaid.

CONCLUSION

We have presented branching fraction measurements for the decays $\overline{B}^0 \to \Lambda_c^+\overline{p}$ and $B^- \to \Lambda_c^+\overline{p}\pi^-$:

$$\begin{aligned}\mathcal{B}(\overline{B}^0 \to \Lambda_c^+\overline{p}) = \\ (1.89 \pm 0.21 \pm 0.06 \pm 0.49) \times 10^{-5}, \\ \mathcal{B}(B^- \to \Lambda_c^+\overline{p}\pi^-) = \\ (3.38 \pm 0.12 \pm 0.12 \pm 0.88) \times 10^{-4}, \end{aligned} \quad (21)$$

where the uncertainties are statistical, systematic, and due to the uncertainty in $\mathcal{B}(\Lambda_c^+ \to pK^-\pi^+)$, respectively. These measurements are based on 383 million $B\overline{B}$ events produced by the SLAC B Factory and recorded by the *BABAR* detector.

If we combine the statistical and systematic uncertainties only, we obtain $\mathcal{B}(\overline{B}^0 \to \Lambda_c^+\overline{p}) = (1.9 \pm 0.2) \times 10^{-5}$, which is consistent with a previous measurement by the Belle Collaboration of $\mathcal{B}(\overline{B}^0 \to \Lambda_c^+\overline{p}) = (2.2 \pm 0.6) \times 10^{-5}$ [30]. Both measurements use the same value for $\mathcal{B}(\Lambda_c^+ \to pK^-\pi^+)$. However, our measurement for the three-body mode, $\mathcal{B}(B^- \to \Lambda_c^+\overline{p}\pi^-) = (3.4 \pm 0.2) \times 10^{-4}$, is significantly larger (by about 4σ) than the previous measurement from Belle $\mathcal{B}(B^- \to \Lambda_c^+\overline{p}\pi^-) = (2.1 \pm 0.3) \times 10^{-4}$ [25]. The Belle Collaboration measurement uses six coarse regions across the $B^- \to \Lambda_c^+\overline{p}\pi^-$ Dalitz plane to correct for variations in efficiency; we use much finer regions and see significant variation near the edges of the Dalitz plane. This difference in efficiency treatment may account for some of the discrepancy between the two results.

One of the main motivations for studying baryonic B-meson decays is to gain knowledge about baryon-antibaryon production in meson decays. We have measured the ratio of the two branching fractions,

$$\frac{\mathcal{B}(B^- \to \Lambda_c^+\overline{p}\pi^-)}{\mathcal{B}(\overline{B}^0 \to \Lambda_c^+\overline{p})} = 15.4 \pm 1.8 \pm 0.3. \quad (22)$$

In this quantity the 26% uncertainty in $\mathcal{B}(\Lambda_c^+ \to pK^-\pi^+)$ cancels in the branching ratio.

We have also measured the fractions of $B^- \to \Lambda_c^+\overline{p}\pi^-$ decays that proceed through a Σ_c resonance:

$$\begin{aligned}\frac{\mathcal{B}(B^- \to \Sigma_c(2455)^0\overline{p})}{\mathcal{B}(B^- \to \Lambda_c^+\overline{p}\pi^-)} = (12.3 \pm 1.2 \pm 0.8) \times 10^{-2}, \\ \frac{\mathcal{B}(B^- \to \Sigma_c(2800)^0\overline{p})}{\mathcal{B}(B^- \to \Lambda_c^+\overline{p}\pi^-)} = (11.7 \pm 2.3 \pm 2.4) \times 10^{-2}. \end{aligned} \quad (23)$$

Assuming no interference with direct decay to $\Lambda_c^+\overline{p}\pi^-$, about 1/4 of $B^- \to \Lambda_c^+\overline{p}\pi^-$ decays proceed through a Σ_c resonance.

The order of magnitude difference between the decay rates of $B^- \to \Lambda_c^+\overline{p}\pi^-$ and two-body decays such as

$\overline{B}^0 \to \Lambda_c^+\overline{p}$, $B^- \to \Sigma_c(2455)^0\overline{p}$, and $B^- \to \Sigma_c(2800)^0\overline{p}$ is consistent with the theoretical description [16] that baryonic B decays are favored when the baryon and antibaryon are close together in phase space. This interpretation is also supported by the observation of the enhancement in rate when $m_{\Lambda_c\overline{p}}$ is near threshold. Although the $\Lambda_c^+\overline{p}$ threshold enhancement alone could indicate a resonance below threshold, enhancements have been observed in other baryon-antibaryon systems and in decays such as $e^+e^- \to p\overline{p}\gamma$ [1, 2]. Therefore the body of measurements indicates that we are observing a phenomenon that is common to baryon production from meson decays, and possibly common to baryon production in general.

We have used the angular distribution of the decay $B^- \to \Sigma_c(2455)^0\overline{p}$ to study the spin of the Σ_c^0 baryon. The helicity angle distribution is consistent with being uniform, which indicates that the Σ_c^0 has $J = 1/2$ assuming the ground state Λ_c^+ also has $J = 1/2$ and excludes the $J = 3/2$ hypothesis at the $> 4\sigma$ level. This is consistent with quark model expectations for the lowest Σ_c baryon state.

We also observe an excited Σ_c state in B-meson decays to $\Lambda_c^+\overline{p}\pi^-$. We measure the mass of this resonance to be $(2846 \pm 8 \pm 10)\,\mathrm{MeV}/c^2$ and the width to be $(86\ ^{+\ 33}_{-\ 22})\,\mathrm{MeV}$. It is possible that this observation is a confirmation of a triplet of $\Sigma_c(2800)$ states seen in $\Lambda_c^+\pi^-$ continuum production [29]. However, the neutral $\Sigma_c(2800)^0$ has a measured mass of $(2802\ ^{+\ 4}_{-\ 7})\,\mathrm{MeV}/c^2$ and width of $(61\ ^{+\ 28}_{-\ 18})\,\mathrm{MeV}$. The widths of the $\Sigma_c(2800)$ and the state observed in B decays are consistent, but the masses are 3σ apart. If these are indeed the same state, then the discrepancy in measured masses needs to be resolved.

Another possible interpretation is that the excited Σ_c^0 resonance seen in this analysis is not the $\Sigma_c(2800)^0$ that was previously observed. A clear signal is evident for $B^- \to \Sigma_c(2455)^0\overline{p}$ decays, but we do not see any evidence for the decay $B^- \to \Sigma_c(2520)^0\overline{p}$. The absence of the decay $B^- \to \Sigma_c(2520)^0\overline{p}$ is in contrast to a claimed 2.9σ signal from an analysis by the Belle Collaboration based on 152 million $B\overline{B}$ events [25]. Also, an examination of the $B^- \to \Lambda_c^+\overline{p}\pi^-$ Dalitz plot shows no evidence for the decay $B^- \to \Lambda_c^+\bar{\Delta}(1232)^{--}$. The $\Sigma_c(2520)^0$ is a well-established state, and so is the $\Delta(1232)^{++}$. Both are expected to have $J = 3/2$. The Belle Collaboration tentatively identified the $\Sigma_c(2800)^0$ as $J = 3/2$ based on the measured mass of the state, while there is weak evidence that the excited Σ_c^0 we observe is $J = 1/2$. It is therefore possible that B decays to higher-spin baryons are suppressed, perhaps due to the same baryon production mechanisms that suppress two-body baryonic decays, and that the excited Σ_c^0 state that we have observed is a newly-observed spin-1/2 state.

We are grateful for the extraordinary contributions of our PEP-II colleagues in achieving the excellent luminosity and machine conditions that have made this work possible. The success of this project also relies critically on the expertise and dedication of the computing organizations that support *BABAR*. The collaborating institutions wish to thank SLAC for its support and the kind hospitality extended to them. This work is supported by the US Department of Energy and National Science Foundation, the Natural Sciences and Engineering Research Council (Canada), the Commissariat à l'Energie Atomique and Institut National de Physique Nucléaire et de Physique des Particules (France), the Bundesministerium für Bildung und Forschung and Deutsche Forschungsgemeinschaft (Germany), the Istituto Nazionale di Fisica Nucleare (Italy), the Foundation for Fundamental Research on Matter (The Netherlands), the Research Council of Norway, the Ministry of Education and Science of the Russian Federation, Ministerio de Educación y Ciencia (Spain), and the Science and Technology Facilities Council (United Kingdom). Individuals have received support from the Marie-Curie IEF program (European Union) and the A. P. Sloan Foundation.

[1] B. Aubert *et al.* (*BABAR* Collaboration), Phys. Rev. D **72**, 051101 (2005).
[2] B. Aubert *et al.* (*BABAR* Collaboration), Phys. Rev. D **74**, 051101 (2006).
[3] E. Barberio *et al.* (Heavy Flavor Averaging Group), hep-ex/0603003 (2006); B. Aubert *et al.* (*BABAR* Collaboration), Phys. Rev. Lett. **97**, 171803 (2006); B. Aubert *et al.* (*BABAR* Collaboration), Phys. Rev. D **72**, 052004 (2005); P. Koppenburg *et al.* (Belle Collaboration), Phys. Rev. Lett. **93**, 061803 (2004); K. Abe *et al.* (Belle Collaboration), Phys. Lett. B **511**, 151 (2001); S. Chen *et al.* (CLEO Collaboration), Phys. Rev. Lett. **87**, 251807 (2001).
[4] M.-Z. Wang *et al.* (Belle Collaboration), Phys. Rev. D **76**, 052004 (2007).
[5] M. Misiak *et al.*, Phys. Rev. Lett. **98**, 022002 (2007); T. Becher and M. Neubert, Phys. Rev. Lett. **98**, 022003 (2007).
[6] C. Q. Geng and Y. K. Hsiao, Phys. Lett. B **610**, 67 (2005); H.-Y. Cheng and K.-C. Yang, Phys. Lett. B **533**, 271 (2002).
[7] H. Albrecht *et al.* (ARGUS Collaboration), Z. Phys. C **56**, 1 (1992).
[8] W.-M. Yao *et al.* (Particle Data Group), J. Phys. **G33**, 1 (2006) and 2007 partial update for the 2008 edition.
[9] M. Jarfi *et al.*, Phys. Rev. D **43**, 1599 (1991).
[10] N. G. Deshpande *et al.*, Mod. Phys. Lett. **A3**, 749 (1988).
[11] P. Ball and H. G. Dosch, Z. Phys. C **51**, 445 (1991).
[12] L. J. Reinders *et al.*, Phys. Rep. **127**, 1 (1985).
[13] V. Chernyak and I. Zhitnitsky, Nucl. Phys. B **345**, 137 (1990).
[14] H.-Y. Cheng and K.-C. Yang, Phys. Rev. D **67**, 034008 (2003).
[15] H.-Y. Cheng and K.-C. Yang, Phys. Rev. D **65**, 054028

(2002).
[16] W.-S. Hou and A. Soni, Phys. Rev. Lett. **86**, 4247 (2001).
[17] Unless specifically stated otherwise, conjugate decay modes are assumed throughout this paper.
[18] B. Aubert *et al.* (*BABAR* Collaboration), Nucl. Instrum. Methods Phys. Res., Sect. A **479**, 1 (2002).
[19] D. J. Lange, Nucl. Instrum. Methods Phys. Res., Sect. A **462**, 152 (2001).
[20] T. Sjostrand *et al.*, J. High Energy Phys. 05, (2006) 026.
[21] S. Agostinelli *et al.* (GEANT4 Collaboration), Nucl. Instrum. Methods Phys. Res., Sect. A **506**, 250 (2003).
[22] R. A. Fisher, Annals Eugen. **7**, 179 (1936).
[23] S. Brandt *et al.*, Phys. Lett. **12**, 57 (1964); E. Farhi, Phys. Rev. Lett. **39**, 1587 (1977).
[24] B. Aubert *et al.* (*BABAR* Collaboration), Phys. Rev. D **71**, 111102(R) (2005).
[25] N. Gabyshev *et al.* (Belle Collaboration), Phys. Rev. Lett. **97**, 242001 (2006).
[26] H. Albrecht *et al.* (ARGUS Collaboration), Z. Phys. C **48**, 543 (1990).
[27] M. Pivk and F. R. Le Diberder, Nucl. Instrum. Methods Phys. Res., Sect. A **555**, 356 (2005).
[28] L. Lyons *et al.*, Nucl. Instrum. Methods Phys. Res., Sect. A **270**, 110 (1988).
[29] R. Mizuk *et al.* (Belle Collaboration), Phys. Rev. Lett. **94**, 122002 (2005).
[30] N. Gabyshev *et al.* (Belle Collaboration), Phys. Rev. Lett. **90**, 121802 (2003).